

Review

Recent Progress in Porphyrin/g-C₃N₄ Composite Photocatalysts for Solar Energy Utilization and Conversion

Sudi Chen ¹, Jiajia Wei ² , Xitong Ren ¹, Keke Song ², Jiajie Sun ^{3,*}, Feng Bai ^{1,*}  and Shufang Tian ^{2,*} 

¹ Key Laboratory for Special Functional Materials of Ministry of Education, National and Local Joint Engineering Research Center for High-Efficiency Display and Lighting Technology, School of Materials Science and Engineering, and Collaborative, Innovation Center of Nano Functional Materials and Applications, Henan University, Kaifeng 475004, China

² Henan International Joint Laboratory of Medicinal Plants Utilization, College of Chemistry and Molecular Science, Henan University, Kaifeng 475004, China

³ School of Physics and Electronics, Henan University, Kaifeng 475004, China

* Correspondence: sunjiajie2006@hotmail.com (J.S.); baifengsun@126.com (F.B.); tianshufang@henu.edu.cn (S.T.)

Abstract: Transforming solar energy into chemical bonds is a promising and viable way to store solar energy. Porphyrins are natural light-capturing antennas, and graphitic carbon nitride (g-C₃N₄) is an effective, artificially synthesized organic semiconductor. Their excellent complementarity has led to a growing number of research papers on porphyrin/g-C₃N₄ hybrids for solar energy utilization. This review highlights the recent progress in porphyrin/g-C₃N₄ composites, including: (1) porphyrin molecules/g-C₃N₄ composite photocatalysts connected via noncovalent or covalent interactions, and (2) porphyrin-based nanomaterials/g-C₃N₄ composite photocatalysts, such as porphyrin-based MOF/g-C₃N₄, porphyrin-based COF/g-C₃N₄, and porphyrin-based assembly/g-C₃N₄ heterojunction nanostructures. Additionally, the review discusses the versatile applications of these composites, including artificial photosynthesis for hydrogen evolution, CO₂ reduction, and pollutant degradation. Lastly, critical summaries and perspectives on the challenges and future directions in this field are also provided.

Keywords: porphyrin; g-C₃N₄; solar energy; hydrogen generation; CO₂ reduction; pollutants degradation



Citation: Chen, S.; Wei, J.; Ren, X.; Song, K.; Sun, J.; Bai, F.; Tian, S.

Recent Progress in Porphyrin/g-C₃N₄ Composite Photocatalysts for Solar Energy Utilization and Conversion. *Molecules* **2023**, *28*, 4283. <https://doi.org/10.3390/molecules28114283>

Academic Editors: Yu G. Gorbunova and Alexander G. Martynov

Received: 6 May 2023

Revised: 17 May 2023

Accepted: 22 May 2023

Published: 23 May 2023



Copyright: © 2023 by the authors. Licensee MDPI, Basel, Switzerland. This article is an open access article distributed under the terms and conditions of the Creative Commons Attribution (CC BY) license (<https://creativecommons.org/licenses/by/4.0/>).

1. Introduction

In recent decades, global energy consumption and demand have grown rapidly alongside population and economic growth. However, the traditional carbon-based fossil energy resources, particularly coal, are facing not only a shortage of reserves but also leading to excessive CO₂ emissions and accumulation in the atmosphere, posing a threat to the environment and ecology. Therefore, developing clean and sustainable new carbon-neutral energy sources has become a pressing scientific challenge. Solar energy is one of the most secure and valuable resources and the largest mineable among all renewable energy sources [1–3]. However, the challenge lies in exploring and storing this abundant resource. One promising approach is to convert solar energy into chemical bonds, such as generating hydrogen and oxygen through water splitting or obtaining reduced fuels like methane, methanol, carbon monoxide, or other hydrocarbon species through CO₂ reduction [4–6]. Additionally, solar energy can be utilized to degrade organic pollutants, thus relieving the pressure of environmental pollution [7,8]. The crux of addressing solar energy utilization and conversion lies in developing photocatalysts with higher artificial photosynthesis or photodegradation efficiency.

The organic semiconductor graphitic carbon nitride (g-C₃N₄), depicted in Figure 1a, featuring heptazine rings (Figure 1b) as fundamental structural units, has undergone extensive research and application in the field of photocatalysis over the past decades [9–11].

This material offers several advantages, which are outlined as: (1) It is non-toxic, low-cost, and easily prepared with a wide range of nitrogen-rich materials as precursors, including melamine, urea, cyanamide, dicyanamide, and thiourea. (2) It possesses suitable bandgap (about 2.7 eV) and responses to visible-light range. The conduction band (CB) and the valence band (VB) of pristine $g\text{-C}_3\text{N}_4$ are commonly located at -1.3 and 1.4 eV, respectively, which sufficiently satisfies the requirements of hydrogen and oxygen generation by splitting water, CO_2 photocatalytic reduction, and organic pollutants degradation from the thermodynamic aspect. Furthermore, in contrast to inorganic semiconductors, the narrow bandgap of $g\text{-C}_3\text{N}_4$ enables it to harvest the sunlight with a wavelength up to 460 nm, which enables it to utilize solar energy more efficiently. (3) Its two-dimensional (2D) lamellar structure with van der Waals between interlayers not only contributes to adsorbing more reactants and exposing more catalytic active sites, but also facilitates post modification, such as exfoliation, to further increase its specific surface area. (4) It is gifted with distinctive surface properties that facilitates hydrogen bonds or to covalently connect with organic molecules for its surface functional groups, such as amines; it tends to form $\pi\text{-}\pi$ stacking with other aromatic molecules due to its conjugated structure; it opts to chelate with metal ion for its electron-rich characters, and so on. (5) Thanks to its unique molecular structure, it is not only provided with excellent thermal and chemical stability even under strong acids and alkali conditions, but can also be modified by means of various organic chemistry methods apart from the strategies generally employed for inorganic semiconductors. Therefore, $g\text{-C}_3\text{N}_4$ has wide application prospects in the field of photocatalysis.

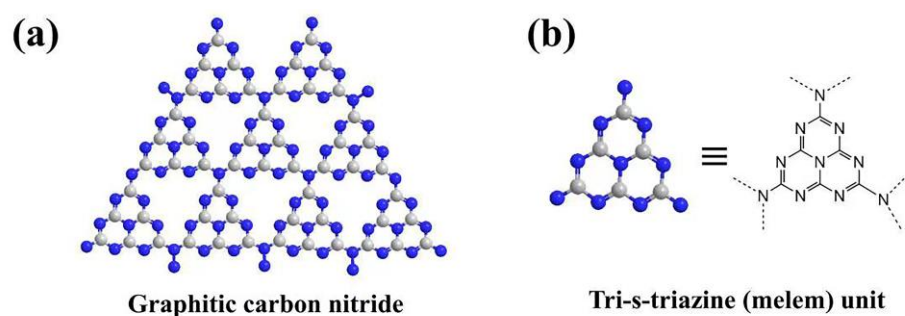


Figure 1. Chemical structure of $g\text{-C}_3\text{N}_4$ (a) and tri-s-triazine (heptazine) (b).

It is unfortunate that $g\text{-C}_3\text{N}_4$ still faces limitations such as a limited visible light response range, a small specific surface area, and rapid recombination of photo-generated charge carriers. Consequently, numerous strategies have been employed to enhance the photocatalytic performance of $g\text{-C}_3\text{N}_4$. These approaches encompass various techniques such as nanostructure design, exfoliation, doping with elements and molecules, and the construction of heterojunctions, such as porphyrin/ $g\text{-C}_3\text{N}_4$ heterojunctions [12,13].

Before delving into porphyrin and porphyrin/ $g\text{-C}_3\text{N}_4$ heterojunctions, it is essential to grasp the concept of the three distinct types of heterojunctions [10,14,15]. In the case of type I band alignment (Figure 2a), semiconductor 1 exhibits a more negative CB and a more positive VB compared to semiconductor 2. When the irradiation light energy equals or exceeds the bandgap of semiconductor 1, the photo-generated electrons or holes tend to migrate to the adjacent CB or VB of semiconductor 2, where charge carriers accumulate. This not only fails to improve the separation efficiency of charge carriers but also diminishes the redox ability. However, in type II band alignment (Figure 2b), the CB and VB potentials are intertwined between semiconductor 1 and semiconductor 2. Photo-induced electrons and holes migrate in opposite directions, creating an internal electric field that enhances the spatial separation of electron-hole pairs and significantly inhibits recombination. Consequently, the oxidation and reduction reaction occur in two semiconductors, but with the diminished redox capacity as a cost. To address this predicament, a Z-scheme heterojunction has been developed. One type is the semiconductor–semiconductor Z-

scheme heterojunction (Figure 2c), where photo-induced electrons from semiconductor 2 interact with the positive edge of semiconductor 1, and both the electrons and holes remain in the CB of semiconductor 1 and the VB of semiconductor 2. The other type is the semiconductor–conductor–semiconductor Z-scheme heterojunction (Figure 2d), where an electron conductor such as a noble metal or graphene bridges the two semiconductors, facilitating electron transmission from semiconductor 2 to semiconductor 1. Moreover, this heterojunction maintains the high redox ability.

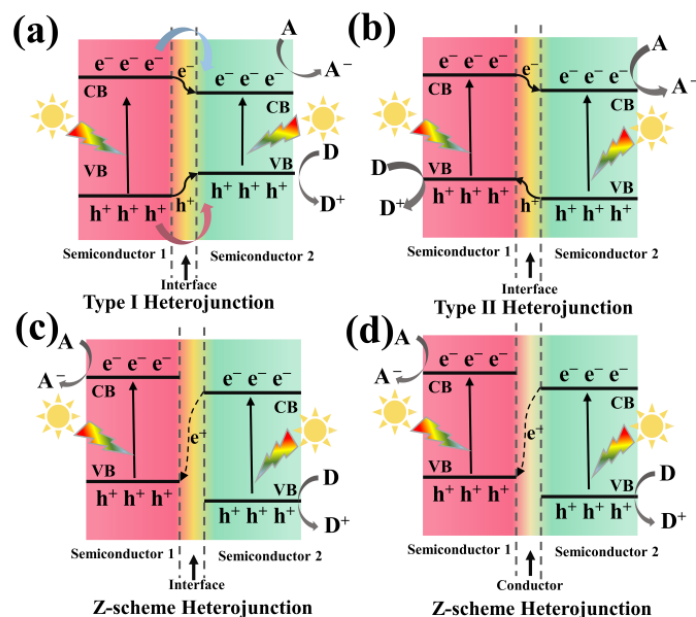


Figure 2. Schematic illustration of the three types of heterojunctions in a semiconductor hybrid: Type I heterojunction (a), Type II heterojunction (b), and Z-scheme heterojunction (c,d).

Porphyrins are a class of heterocyclic macromolecules with a rigid skeleton (porphin, depicted in Figure 3a) and a highly π -conjugated system. They are widely found in nature (heme and chlorophyll, as shown in Figure 3b,c) and play a crucial role in essential biological processes such as photosynthesis, oxygen transport, and redox reactions [16,17]. In the photosynthesis process, porphyrins and their derivatives serve as chromophores, absorbing solar energy and converting it into chemical energy. Due to their advantageous features, including excellent redox properties, remarkable visible light harvesting capacity (with extinction coefficient of approximately $10^5 \text{ L}\cdot\text{mol}^{-1}\cdot\text{cm}^{-1}$) [17], high emission intensity, moderate stability, ease of structural modification and functionalization, a wide range of porphyrin-based photocatalysts have been developed, exhibiting captivating optical properties and promising photocatalytic performance [18]. However, as molecular catalysts, porphyrins face certain limitations, such as photo-corrosion under prolonged light irradiation and difficulties in recycling once the reaction is complete. One feasible strategy to address these challenges is to combine g- C_3N_4 with porphyrin. This hybrid approach allows for the simultaneous mitigation of the weaknesses associated with g- C_3N_4 and porphyrin. Firstly, the exceptional photosensitivity of porphyrin significantly expands the range of visible light absorption. Secondly, the highest occupied molecular orbital (HOMO) and lowest unoccupied molecular orbital (LUMO) positions of porphyrin align well with the band structure of g- C_3N_4 (as shown in Figure 4a), thereby facilitating the separation and transmission of charge carriers. Additionally, the strong interface interaction between the two components establishes efficient electron transfer pathways and reduces the migration distance (as depicted in Figure 4b). Lastly, the copolymerization strategy employed to combine porphyrin and g- C_3N_4 can optimize the properties of g- C_3N_4 , such as its specific surface area, as the introduction of porphyrin as a comonomer alters the original polymerization pathway.

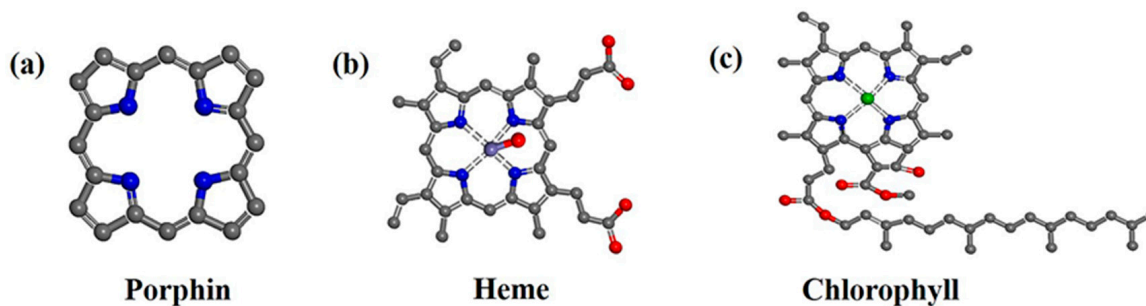


Figure 3. Chemical structure of porphin (a), heme (b), and chlorophyll (c).

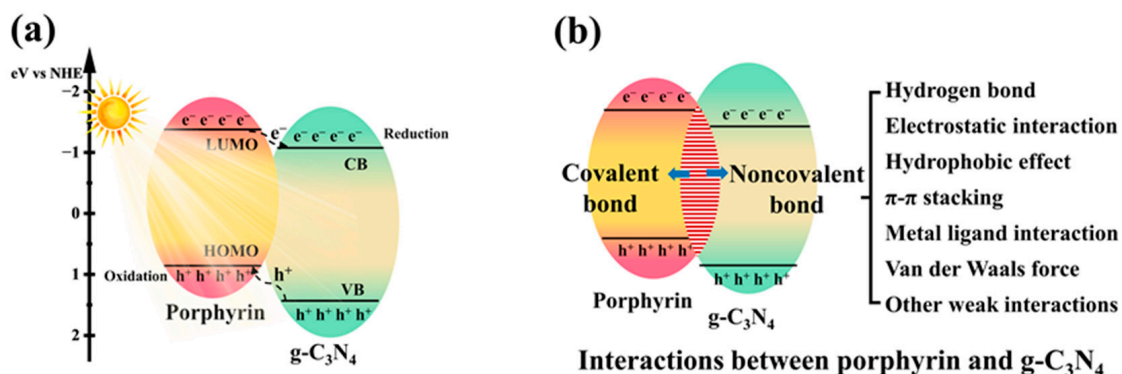


Figure 4. Schematic illustration of the energy band diagram (a) and interactions (b) between porphyrin and $g-C_3N_4$.

The porphyrin/ $g-C_3N_4$ hybrid materials are anticipated to demonstrate superior photocatalytic performance compared to their individual components. Significantly, substantial progress has been achieved in recent years. This review (Figure 5) focuses on the fabrication of these composites and their application in solar energy utilization and conversion, which includes photocatalytic hydrogen generation, CO_2 reduction, and pollutant degradation. Ultimately, conclusions and further prospects on the porphyrin/ $g-C_3N_4$ composites are put forward, which would accelerate the deeper understanding and the more extensive application of the porphyrin/ $g-C_3N_4$ composites for solar energy utilization.

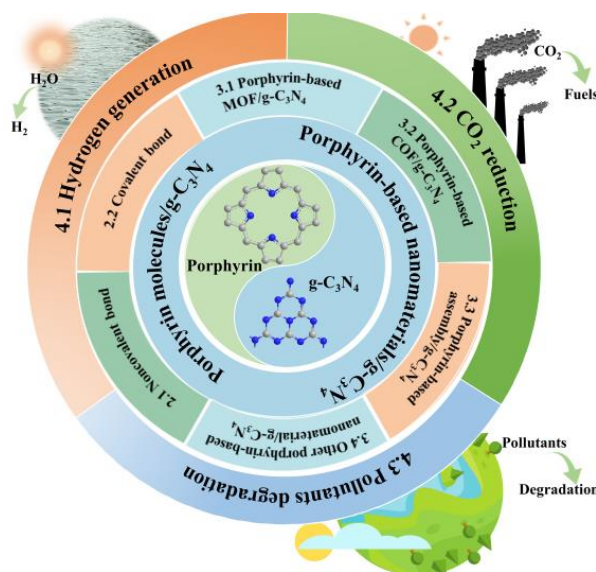


Figure 5. Schematic illustration of the framework and the sections of this review.

2. Fabrication of Porphyrin Molecules/g-C₃N₄ Composite Photocatalysts

A series of porphyrin molecules/g-C₃N₄ composites have been prepared to date and have exhibited improved photocatalytic activity compared to pristine g-C₃N₄, and the research showed that the properties and the photocatalytic activities are all clearly impacted by the interactions between porphyrin molecules and g-C₃N₄.

2.1. Noncovalent Bond Interactions between Porphyrin Molecules and g-C₃N₄

Noncovalent bond interactions mainly include hydrogen bonds, electrostatic interaction, hydrophobic effect, π - π stacking, metal ligand interaction, van der Waals force, and other weak interactions. Porphyrin molecules and g-C₃N₄ both possess conjugated structures with abundant surface functional groups, it is easy to compound these two together. The Yao group [19] successfully fabricated a pure organic heterostructure of g-C₃N₄/ μ -oxo dimeric iron(III) porphyrin [(FeTPP)₂O] (Figure 6) through π - π stacking and Fe-amine interactions. This was made possible due to the flexible 2D structure and ample amine groups present in g-C₃N₄. The experiment demonstrated that the porphyrin (FeTPP)₂O not only acted as a photosensitizer but also served as a charge promoter, effectively suppressing the recombination of photo-induced electrons and holes in g-C₃N₄. Li et al. [20] utilized different asymmetric zinc porphyrin (ZnPy) molecules as photosensitizers, adsorbing them onto the surface of g-C₃N₄ (Figure 7). The results revealed that porphyrin molecules with three 3-pyridine substitutions exhibited significantly enhanced photocatalytic activity and stability on Pt/g-C₃N₄ compared to those with three phenyl groups. The observed differences were mainly attributed to the rapid electron transfer between porphyrin molecules containing pyridine groups and g-C₃N₄. In another study by the Yan group [21], tetra(4-carboxyphenyl) porphyrin (TCPP) was loaded onto the surface of Pt/g-C₃N₄ through a simple adsorption process, resulting in the composite TCPP/Pt/g-C₃N₄. This organic heterostructure not only improved visible light utilization but also facilitated efficient electron transfer while suppressing the recombination of photo-induced charge carriers. The g-C₃N₄/FeTCPP heterogeneous catalyst was prepared by the He group [22] using a straightforward self-assembly approach. In addition to π - π stacking, the interaction between the carboxyl group of FeTCPP and the abundant amino groups of g-C₃N₄ formed hydrogen bonds, as illustrated in Figure 8. The resulting g-C₃N₄/FeTCPP photocatalysts exhibited remarkable activity in CO₂ reduction, with a CO evolution rate exceeding 1 mmol g⁻¹ h⁻¹ and a selectivity of 98%. Zhao et al. [23] conveniently immobilized cobalt meso-tetra-phenylporphyrin (CoTPP) onto g-C₃N₄ through π - π supramolecular interaction via self-assembly. The pores induced by the π - π stacking of g-C₃N₄ and CoTPP also provided ample space for CO₂ adsorption. CoTPP demonstrated excellent CO₂ photoelectrocatalytic activity, characterized by low overpotential and long-term stability. Formic acid was generated as a liquid reduction product, exhibiting a prominent TON value and high selectivity of nearly 100%. To study the effect of carboxyl groups and their peripheral position on H₂ generation from water splitting [24], free-base porphyrins (TPP, *m*TCPP, *p*TCPP) were used to sensitize g-C₃N₄ hybrid photocatalysts through impregnation via noncovalent interactions. All the hybrids displayed enhanced photocatalytic performance for hydrogen evolution compared to pure g-C₃N₄. Zhu et al. [25] synthesized a series of photocatalysts by combining g-C₃N₄ with metal-porphyrins (MTPPs) through a facile solvothermal method. Notably, CoTPP/g-C₃N₄ exhibited excellent activity in the photodegradation of rhodamine B (RhB) when compared to pure g-C₃N₄. The enhanced photocatalytic activity was attributed to the more effective interfacial charge transfer between CoTPP and g-C₃N₄. The Zhu group [26] synthesized a series of naphthalimide-porphyrin (NP)/g-C₃N₄ hybrids, where planar NP molecules were adsorbed onto the 2D g-C₃N₄ through π - π stacking. The introduction of NP efficiently inhibited charge recombination and facilitated Förster energy transfer from the donor (g-C₃N₄) to the acceptor (NP) due to the overlap between the absorption spectrum of NP and the emission of g-C₃N₄. As a result, the photocatalytic hydrogen production performance of 2%NP/g-C₃N₄ surpassed that of ZnTCPP/g-C₃N₄ and ZnTPP/g-C₃N₄. The Abrahamsson group [27] prepared a hybrid assembly of carbon

nitride quantum dots (CNQDs) and Fe-porphyrin (Fe-p-TMA), where CNQDs functioned as a visible light absorber and Fe-p-TMA acted as the catalyst for CO₂ to CO conversion. The interactions between CNQDs and Fe-porphyrin involved electrostatic forces and π - π stacking, establishing a more direct charge transfer pathway that greatly facilitated the CO₂ to CO transformation.

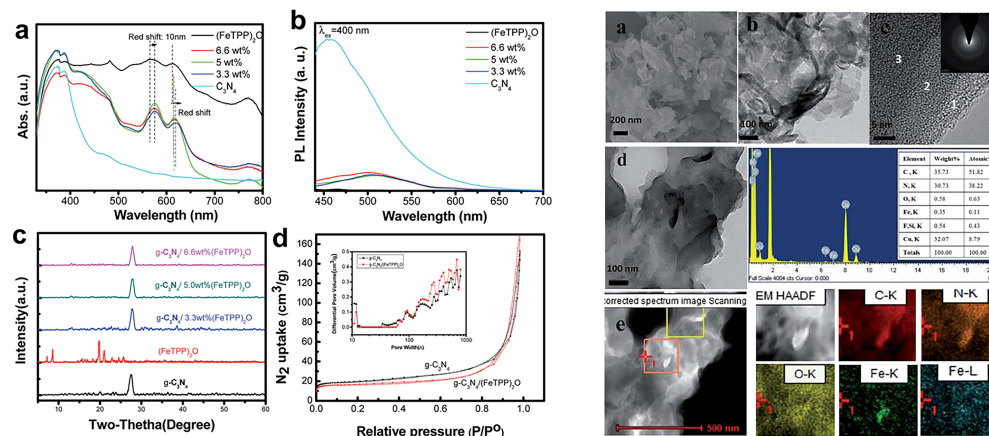


Figure 6. UV-vis diffuse reflection spectra (a), photoluminescence spectra (b), XRD patterns (c), nitrogen adsorption-desorption isotherms (d) of g-C₃N₄, (FeTPP)₂O and g-C₃N₄/(FeTPP)₂O composites (left) and SEM (a), TEM (b), HRTEM (c) images and SAED pattern, TEM images (d) and the corresponding EDS (e), mapping images of the g-C₃N₄/(FeTPP)₂O heterostructure (right). Reproduced from [19] with permission from [Royal Society of Chemistry].

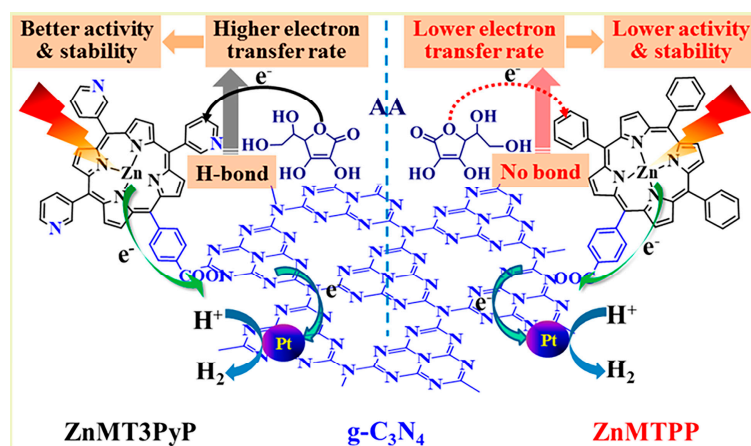


Figure 7. ZnMT₃PyP and ZnMTTP sensitized graphitic carbon nitride for efficient visible light driven H₂ production. Reproduced from [20] with permission from [American Chemical Society].

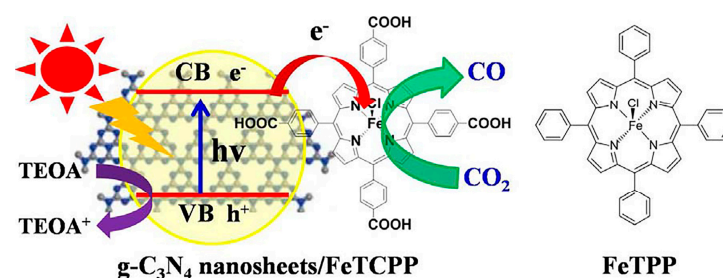


Figure 8. Structure of g-C₃N₄/FeTCPP heterogeneous catalyst system and FeTPP. Reproduced from [22] with permission from [Elsevier].

In addition to the aforementioned two-component hybrids, several tricomponent composites based on porphyrin/ $g\text{-C}_3\text{N}_4$ have also been synthesized. The Li group [28,29] reported copper-bridged $g\text{-C}_3\text{N}_4$ /porphyrin nanocomposites (Figure 9) for enhanced photocatalytic hydrogen generation. In this composite, porphyrin served as visible light absorption antennas, while $g\text{-C}_3\text{N}_4$ acted as a substrate. The introduction of copper at the interface of $g\text{-C}_3\text{N}_4$ and porphyrin not only regulated the morphology and structure of the nanocomposite but also strengthened the interaction between $g\text{-C}_3\text{N}_4$ and porphyrin. This facilitated effective electron transfer, resulting in a significant enhancement of the photocatalytic activity. The He group [30] synthesized the hybrid photocatalyst $g\text{-C}_3\text{N}_4\text{-C}_{0.05}/\text{FeTCPP}$ (Figure 10), where $g\text{-C}_3\text{N}_4$ incorporated with carbon dots acted as the photosensitizer and FeTCPP served as the molecular catalyst. The introduction of trace amounts of carbon dots provided an alternative channel for electron transfer, promoting interfacial charge separation. This resulted in improved photocatalytic performance. Wang et al. [31] fabricated a Z-scheme system, Au-P/Fe-CN (Figure 11), by creating a strong interfacial contact through electrostatic interaction and proper band alignment. The deposition of Au nanoparticles over the surface of P/Fe-CN promoted surface redox properties by enhancing charge carrier separation and transfer efficiency. Multiporphyrin@ $g\text{-C}_3\text{N}_4$ was prepared [32] by binding multi-porphyrin arrays onto the surface of oxidized $g\text{-C}_3\text{N}_4$, which bears plenty of hydroxyl and carboxyl functional groups. PdCl_4^{2-} was employed as a connector in this composite. The experimental results demonstrated that the porphyrin molecules not only acted as photosensitizers but also functioned as charge promoters, reducing the recombination of excited electrons and holes in $g\text{-C}_3\text{N}_4$.

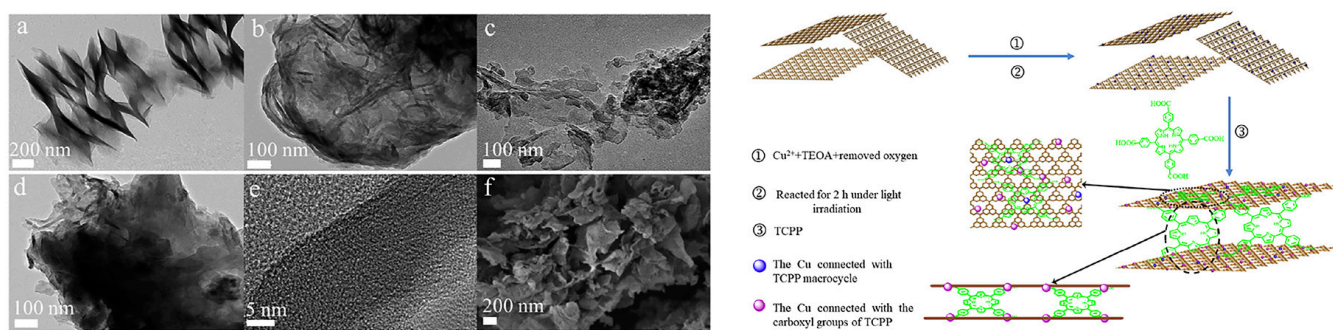


Figure 9. TEM images of TCPP (a), pure $g\text{-C}_3\text{N}_4$ (b), $g\text{-C}_3\text{N}_4\text{-TCPP}$ (c), and $g\text{-C}_3\text{N}_4\text{-Cu-TCPP}$ (d), high resolution transmission electron microscopy image (e) and SEM image (f) of the $g\text{-C}_3\text{N}_4\text{-Cu-TCPP}$ (left), and the formation scheme of the $g\text{-C}_3\text{N}_4\text{-Cu-TCPP}$ composite (right). Reproduced from [28] with permission from [Elsevier].

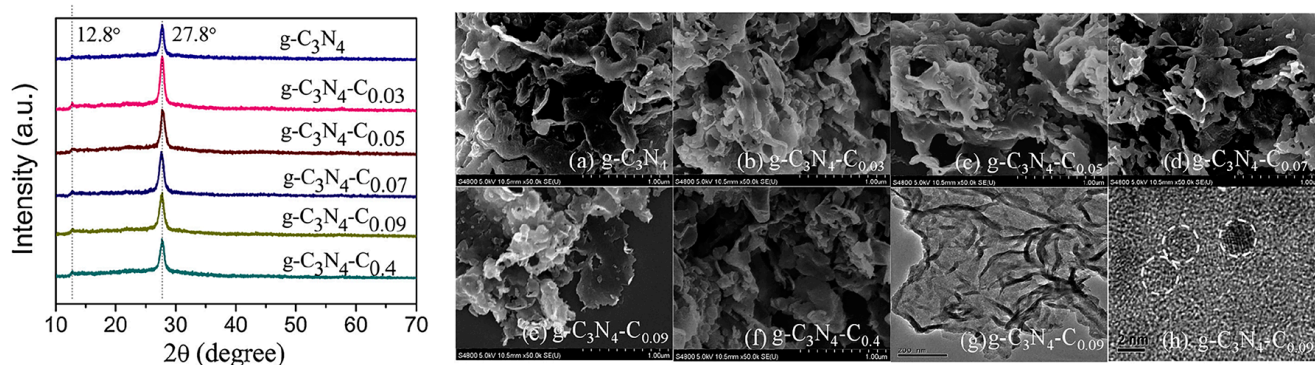


Figure 10. XRD patterns (left), SEM, TEM, and HR-TEM images (right) of as-synthesized $g\text{-C}_3\text{N}_4\text{-C}_x$ ($x = 0\sim 0.4$) samples. Reproduced from [30] with permission from [Elsevier].

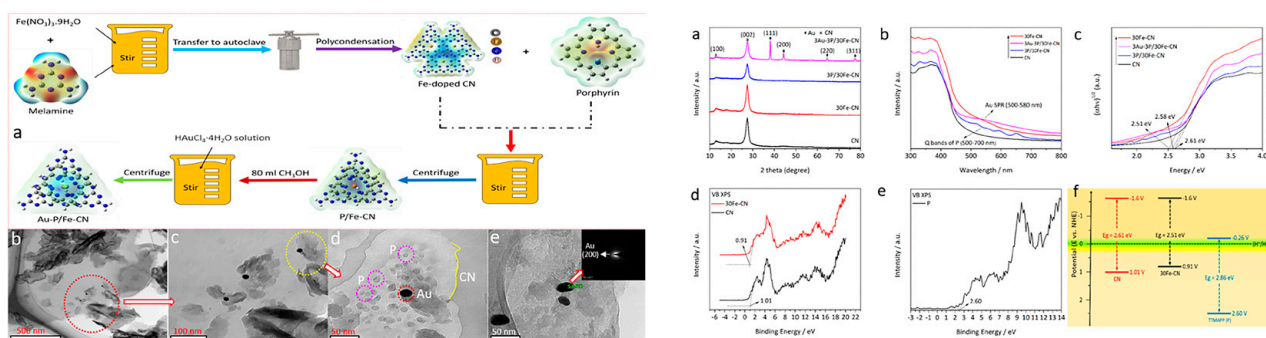


Figure 11. Scheme for the synthesis (a), TEM (b–d), and HR-TEM (e) images of 3Au-3P/30Fe-CN photocatalyst (left), XRD patterns (a), absorption spectra (b), and energy band diagram (c–f) of the as-synthesized photocatalyst samples (right). Reproduced from [31] with permission from [Elsevier].

2.2. Covalent Bond Interactions between Porphyrin Molecules and $g\text{-C}_3\text{N}_4$

As we are aware, the efficiency of electron separation and transmission increases with the strengthening of the interaction between porphyrin and $g\text{-C}_3\text{N}_4$. Considering $g\text{-C}_3\text{N}_4$ as an organic polymeric semiconductor, it is feasible to establish a covalent bond connection with porphyrin, which would significantly enhance electron transfer. The Ye group [33] was the first to report a hybrid composite of covalently linked Co-porphyrin and low-molecular-weight $g\text{-C}_3\text{N}_4$. In this composite, Co-porphyrin acted as the reaction center, while $g\text{-C}_3\text{N}_4$ served as a visible light harvesting antenna. The efficient transmission and accumulation of electrons by the active Co centers, along with the affinity of Co-porphyrin for CO_2 , contributed to the superior photocatalytic performance. This research revolutionized the traditional semiconductor-cocatalyst composite approach.

Post-synthetic modification represents another common approach to covalently link porphyrin with $g\text{-C}_3\text{N}_4$, taking advantage of the abundant amine groups present at the edges of $g\text{-C}_3\text{N}_4$ nanosheets. The construction of a ZnTCPP-sensitized $g\text{-C}_3\text{N}_4$ composite, ZnTCPP/ $g\text{-C}_3\text{N}_4$ (Figure 12), was achieved [34], where ZnTCPP was condensed onto the surface of $g\text{-C}_3\text{N}_4$ through amide groups serving as bridging units. The significantly enhanced photocatalytic performance of this composite was attributed to the highly efficient separation of electron-hole pairs and the promotion of solar energy utilization, both resulting from the introduction of ZnTCPP via covalent connection.

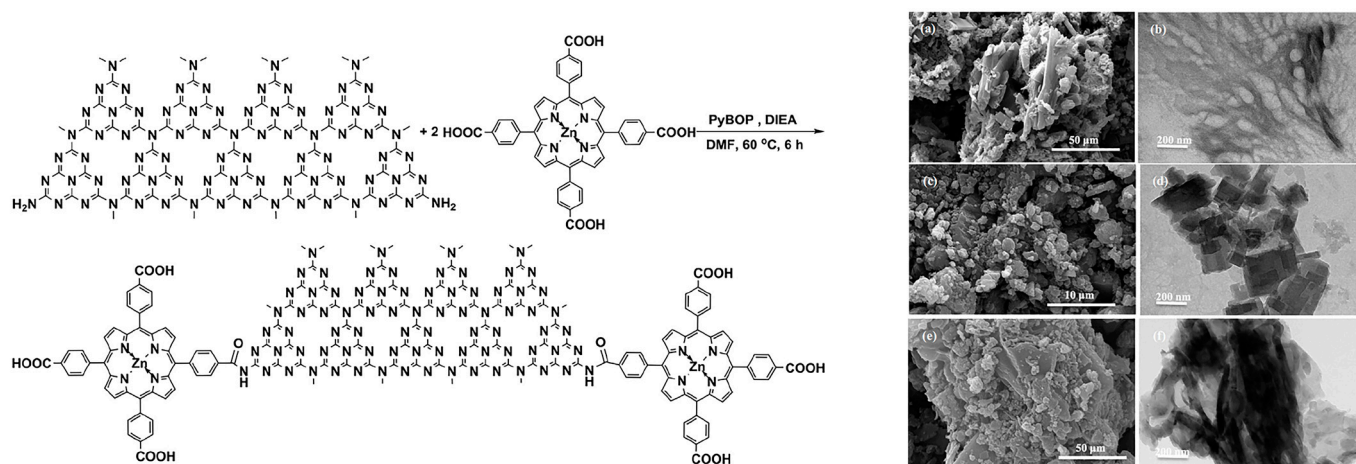


Figure 12. Synthesis of ZnTCPP/ $g\text{-C}_3\text{N}_4$ composites (left), and SEM (a,c,e) and TEM (b,d,f) images of $g\text{-C}_3\text{N}_4$, ZnTCPP, and ZnTCPP/ $g\text{-C}_3\text{N}_4$ (right). Reproduced from [34] with permission from [Elsevier].

Although covalent interactions between porphyrin and $g\text{-C}_3\text{N}_4$ can enhance the separation of photo-induced charges through post-synthetic modification, they do not address the limitations of $g\text{-C}_3\text{N}_4$, such as its limited specific surface area. Copolymerization, however, is a universal strategy for incorporating small organic molecules with suitable functional groups into the $g\text{-C}_3\text{N}_4$ framework. Building upon this approach, 5,10,15,20-tetrakis(4-(2,4-diamino-1,3,5-triazinyl) phenyl)porphyrin (TDPP) and the corresponding metal porphyrin (MTDPP) were designed and synthesized [35,36] as co-monomers to copolymerize with urea, enabling the construction of covalently connected porphyrin and $g\text{-C}_3\text{N}_4$ (Figure 13). The resulting photocatalysts, $g\text{-CNU-TDPP}$ and $g\text{-CNU-MTDPP}$, not only exhibited an expanded absorption range of visible light but also demonstrated an enlarged specific surface area. Additionally, the separation efficiency of photo-generated electron-hole pairs was significantly improved due to the presence of covalent bonds between TDPP, MTDPP, and $g\text{-C}_3\text{N}_4$.

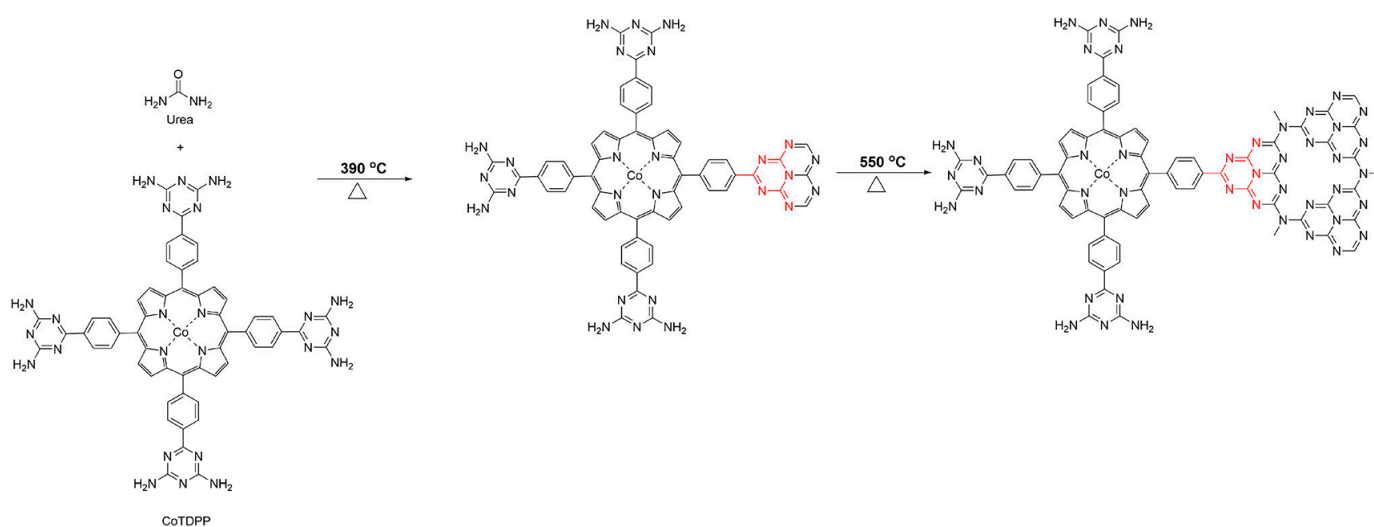


Figure 13. The covalent interaction between CoTDPP and $g\text{-C}_3\text{N}_4$. Reproduced from [36] with permission from [Springer].

3. Fabrication of Porphyrin-Based Nanomaterials/ $g\text{-C}_3\text{N}_4$ Composite Photocatalysts

Various nanomaterials based on porphyrin, such as metal-organic frameworks (MOFs), covalent organic frameworks (COFs), and assemblies, have been successfully fabricated [37–47] owing to their abundant functional groups and conjugated rigid planar structure. In addition to porphyrin molecules/ $g\text{-C}_3\text{N}_4$ hybrids, a wide range of porphyrin-based nanomaterials/ $g\text{-C}_3\text{N}_4$ composites have also been developed for solar energy utilization and conversion.

3.1. Porphyrin-Based MOF/ $g\text{-C}_3\text{N}_4$ Hybrids for Solar Energy Utilization and Conversion

The unique symmetrical macro-ring structure of porphyrin, combined with its different functional substituents, makes it a prominent ligand for coordinating with metal ions to construct highly stable and porous MOF materials with rich pore structures [48–52]. These MOFs find wide applications in catalysis. Moreover, porphyrin-based MOFs combined with $g\text{-C}_3\text{N}_4$ for photocatalysis have been extensively studied. A novel hybrid material was prepared [53] by combining zero-dimensional (0D) carbon nitride quantum dots ($g\text{-CNQDs}$) with 2D ultrathin porphyrin through coordination interactions (Figure 14). This hybrid material exhibited shortened migration pathways for photo-induced electrons and gaseous substrates from $g\text{-CNQDs}$ to Co active sites. The efficient separation of electron-hole pairs and the long-term capture of electrons at Co centers contributed to the photocatalytic activity and selectivity of the hybrid catalyst. In another study by Zhao group [54], a hybrid photocatalyst was constructed by compounding 2D Cu-porphyrin MOF with $g\text{-C}_3\text{N}_4$

via π - π stacking. This photocatalyst exhibited outstanding selectivity in CO_2 reduction under aerobic conditions. The interaction between the 2D-MOF and $g\text{-C}_3\text{N}_4$ resulted in the formation of a type II heterojunction, where photo-induced holes migrated to the $g\text{-C}_3\text{N}_4$ moiety while electrons moved to the 2D-MOF unit. Li et al. [55] developed a heterojunction PCN-222/ $g\text{-C}_3\text{N}_4$ (Figure 15) through a facile one-pot solvothermal approach. The hybrid material showed a broadened light response range, enhanced separation efficiency of photo-generated carriers, and improved adsorption capacity for organic pollutants, leading to superior photocatalytic activity. In the work by Shi group [56], a 2D/2D hybrid photocatalyst was fabricated by combining acidified boron-doped $g\text{-C}_3\text{N}_4$ (HBCNN) with cobalt porphyrin MOF through coordination connections. The interfacial Co-N bond formed a pseudo-gap in the up-spin channel of electronic states, promoting efficient electron-hole separation. The Li group [57] developed a 2D/2D $g\text{-C}_3\text{N}_4$ /PMOF nanohybrid utilizing the interfacial linking of cobalt ions. The presence of cobalt ions with various oxidation states facilitated charge separation and enhanced photocatalytic activity. The sensitization of PMOF resulted in an extended visible light absorption range, while the close and extensive contact at the 2D interface further contributed to the increased photocatalytic performance.

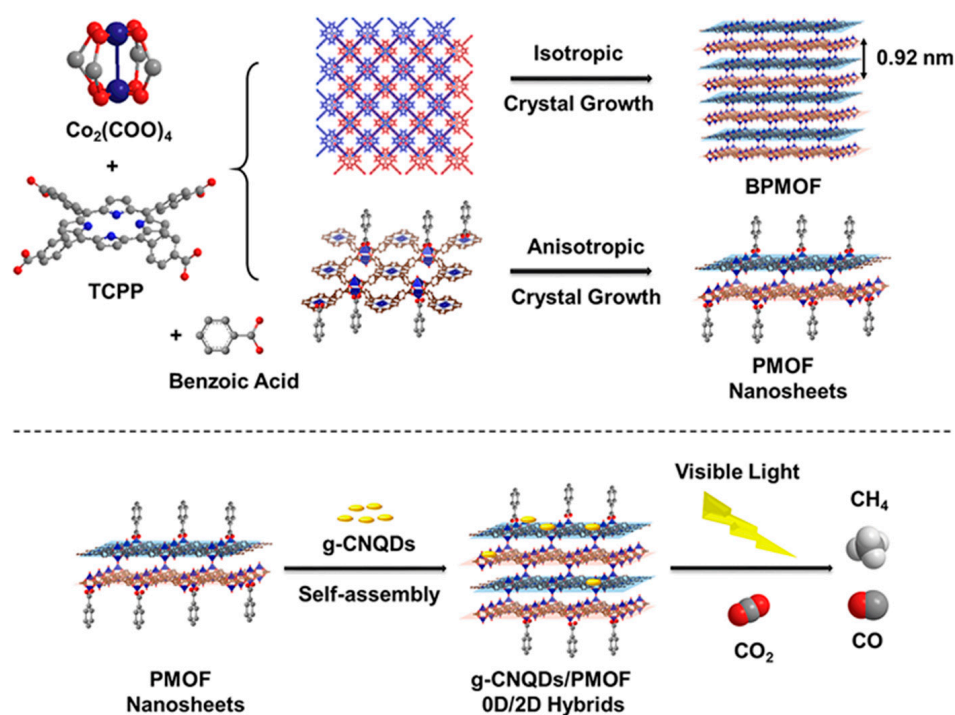


Figure 14. 2D PMOF hybrids with $g\text{-C}_3\text{N}_4$ through coordination interaction. Reproduced from [53] with permission from [American Chemical Society].

3.2. Porphyrin-Based COF/ $g\text{-C}_3\text{N}_4$ Hybrids for Solar Energy Utilization and Conversion

2D COFs are an enchanting class of materials that possess large π -systems and can be easily functionalized with various substituents. Porphyrin, with its easily modifiable structure, is a natural choice as a monomer for synthesizing COFs. The π -stacking aromatic subunits of porphyrin-based COFs provide a convenient pathway for electronic transport between layers. In Figure 16, a 2D heterojunction of porphyrin COFs/ $g\text{-C}_3\text{N}_4$ was created through the in-situ synthesis of CuPor-Ph-COF on the surface of $g\text{-C}_3\text{N}_4$ using a benign liquid-assisted grinding approach [58]. This method effectively reduced the recombination of photogenerated electron-hole pairs and facilitated faster separation of photo-induced charges. As a result, the photocatalyst exhibited superior catalytic performance compared to pure $g\text{-C}_3\text{N}_4$.

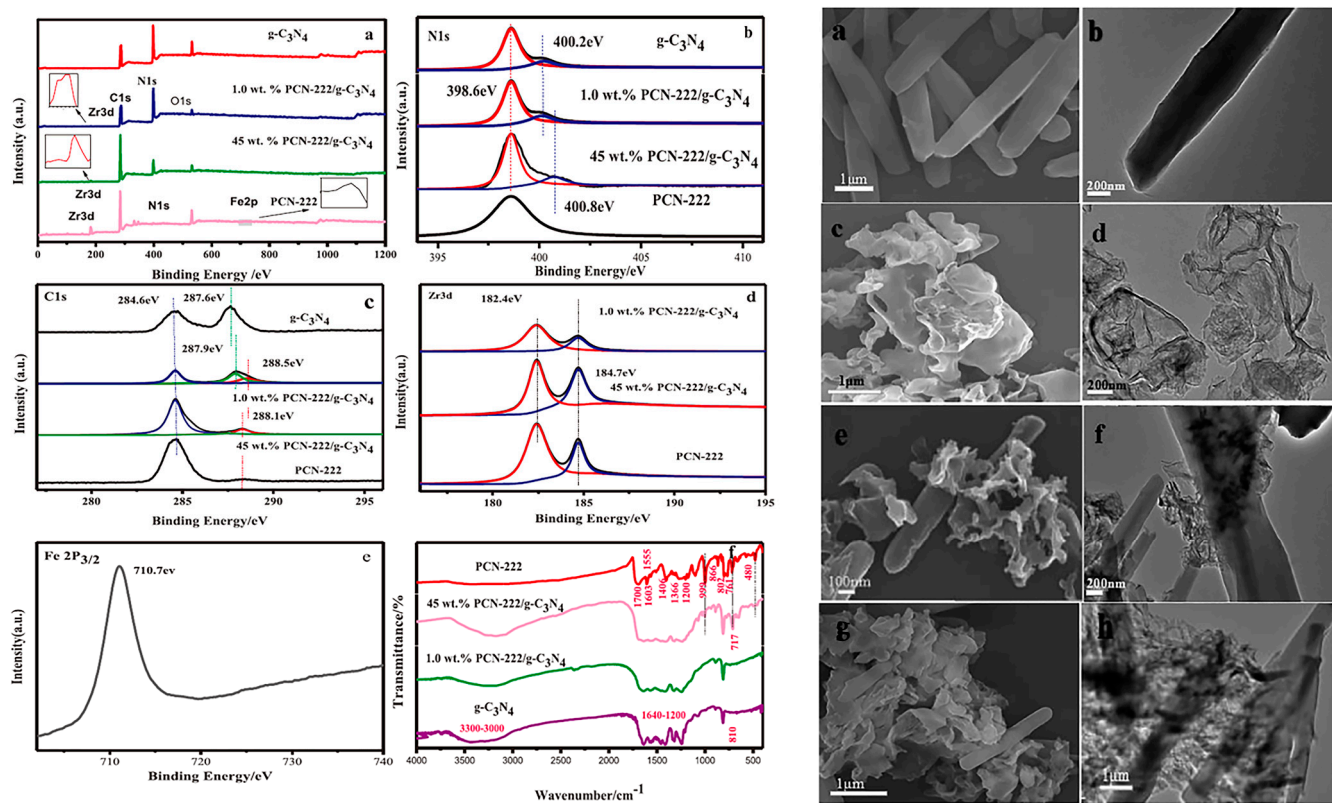


Figure 15. High-resolution XPS (a–d) and FT-IR (e,f) spectra (left), and SEM (a,c,e,g) and TEM (b,d,f,h) images of PCN-222, $g\text{-C}_3\text{N}_4$, and PCN-222/ $g\text{-C}_3\text{N}_4$ (right). Reproduced from [55] with permission from [Elsevier].

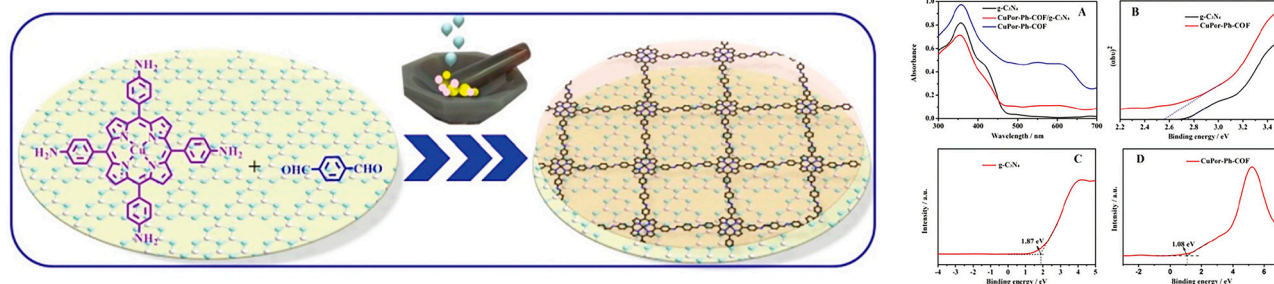


Figure 16. The preparation of CuPor-Ph-COF/ $g\text{-C}_3\text{N}_4$ by the liquid-assisted grinding approach (left), and UV-vis diffuse reflection spectra (A), band gap (B–D) of $g\text{-C}_3\text{N}_4$ and CuPor-Ph-COF/ $g\text{-C}_3\text{N}_4$ (right). Reproduced from [58] with permission from [Royal Society of Chemistry].

3.3. Porphyrin-Based Assembly/ $g\text{-C}_3\text{N}_4$ Hybrids for Solar Energy Utilization and Conversion

Porphyrin serves as a natural building block for constructing well-defined assemblies through various noncovalent interactions, such as $\pi\text{-}\pi$ stacking, electrostatic interactions, coordination bonding, hydrogen bonding, and other van der Waals forces. The self-assembly of porphyrin molecules into ordered spatial arrangements not only expands the absorption range of visible light but also enhances photo-induced electron transmission and improves photostability under long-term irradiation. In a study by the Zhu group [59], an all-organic, self-assembled heterojunction photocatalyst, consisting of TCPP (SA-TCCP) and oxidized $g\text{-C}_3\text{N}_4$ (O-CN), was synthesized using an in situ electrostatic approach (Figure 17). The light-harvesting capacity of O-CN was greatly enhanced by the broad-spectrum responsive ability of SA-TCCP. The $\pi\text{-}\pi$ interaction between SA-TCCP and O-CN facilitated electron delocalization, while the well-matched band structures generated a built-in electric field,

promoting interfacial charge transfer. The synergistic effects between SA-TCCP and O-CN contributed to the enhanced photocatalytic oxidation activities. Kuang et al. [60] designed a heterojunction C_3N_4 -supramolecular TCCP nanosheet (NS) (Figure 18) with efficient charge separation based on van der Waals forces. The porphyrin NS acted as a water oxidation booster, while the C_3N_4 NS synergistically functioned as the CO_2 reduction center. The TCCP- C_3N_4 heterojunction regulated charge migration properties and accelerated robust water oxidation kinetics, thereby enhancing the photocatalytic CO_2 reduction activity. Furthermore, a TCCP nanofibers/ $g-C_3N_4$ nanocomposite was fabricated [61] using a self-assembly approach. The charge separation efficiency was improved through an enhanced exciton-coupled charge transfer process between TCCP aggregates and $g-C_3N_4$. Additionally, the optimized capture capacity of photon energy contributed to the promoted photodegradation efficiency.

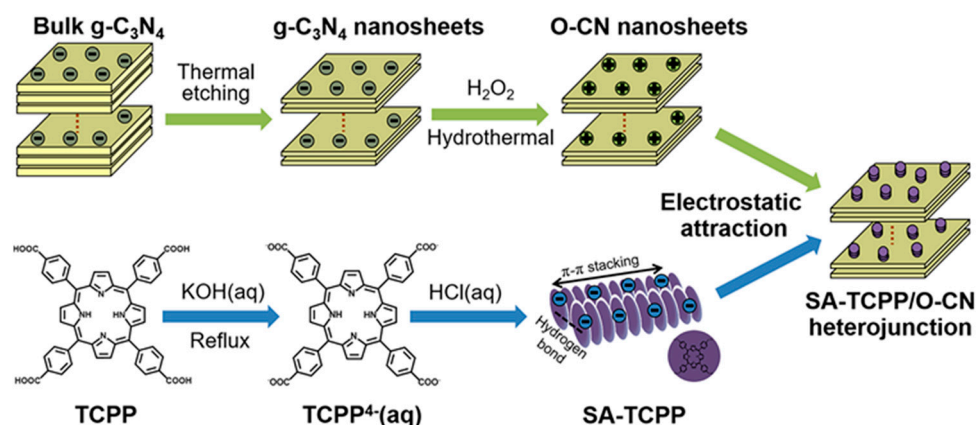


Figure 17. Self-assembly TCCP compound with oxidized $g-C_3N_4$ via electrostatic interaction. Reproduced from [59] with permission from [Elsevier].

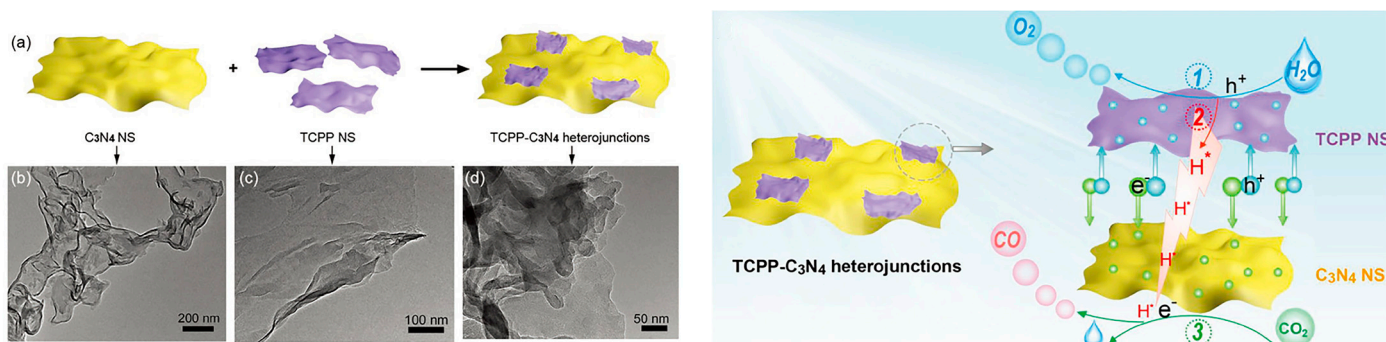


Figure 18. Schematic illustration (a) of the construction of TCCP- C_3N_4 heterojunctions and the corresponding TEM (b–d) images (left), schematic illustration (of the reaction mechanism on TCCP- C_3N_4 heterojunctions (right). Reproduced from [60] with permission from [Wiley].

3.4. Other Porphyrin-Based Nanomaterial/ $g-C_3N_4$ Hybrids for Solar Energy Utilization and Conversion

Except for the aforementioned porphyrin/ $g-C_3N_4$ hybrids, there are additional nanomaterials based on porphyrin coupled with $g-C_3N_4$ that are utilized for solar energy applications. In a study conducted by the Ji group [62], a zinc porphyrin polymer/ $g-C_3N_4$ heterojunction (Figure 19) was reported for photocatalytic synthesis. The hybrid photocatalyst performance was enhanced by the improved visible-light harvesting ability and photo-induced charge mobility resulting from the incorporation of zinc-porphyrin-conjugated microporous polymer. Another photocatalyst, a porphyrin-based metal-organic cages (MOC)/ $g-C_3N_4$ heterostructure, was prepared [63] through π - π stacking to facilitate photocatalytic hydrogen generation in a direct Z-scheme configuration. The direct

Z-scheme heterostructure promoted charge transmission, expanded the light absorption range, protected the cages from degradation within the hybrid, and ultimately enhanced the photocatalytic activity of the system.

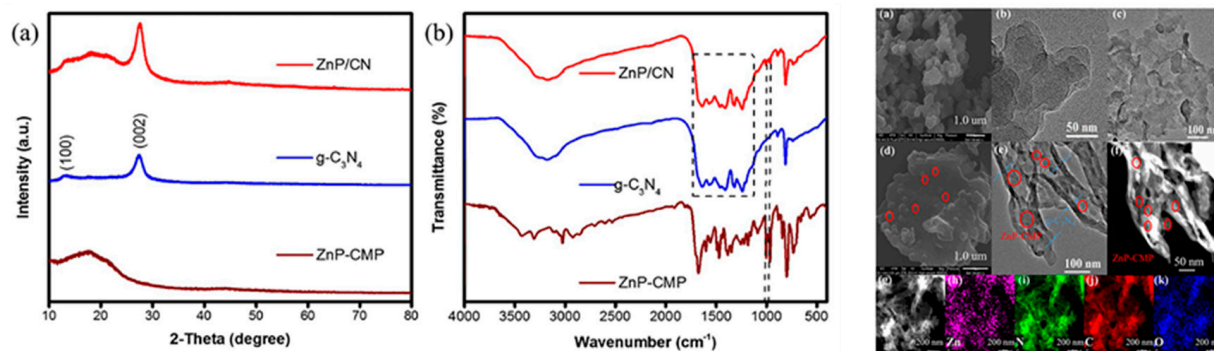


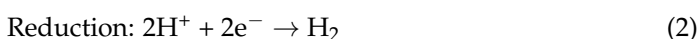
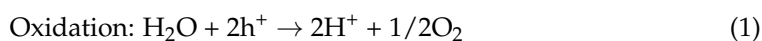
Figure 19. XRD patterns (a) and FT-IR (b) spectra of ZnP/CN, g-C₃N₄, and ZnP-CMP (left), SEM (a,d), TEM (b,c,e,f), and element mapping (e–k) images of ZnP/CN, g-C₃N₄, and ZnP-CMP (right). Reproduced from [62] with permission from [Elsevier].

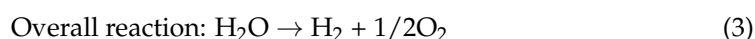
4. Photocatalytic Applications of Porphyrin/g-C₃N₄ Composite for Solar Energy Utilization and Conversion

Due to their potential applications in solar energy utilization and conversion, semiconductor-based photocatalysts have garnered significant attention in the field of energy and the environment. Photocatalytic reactions typically involve three steps [64–66]: (1) Generation of charge carriers: when semiconductors absorb light with energy equal to or greater than their corresponding bandgaps, photocarriers are generated. Excited by photons, electrons (e⁻) move from the valence band (VB) to the conduction band (CB), creating positively charged holes (h⁺) in the VB. The redox abilities of electrons and holes are determined by the positions of the CB and VB. (2) Migration of charge carriers: within the semiconductor, some charge carriers recombine due to defects, collisions, and other factors, while others migrate to the surface of the semiconductor. (3) Involvement of charge carriers in reactions: active electrons or holes on the surface of the semiconductor, either with or without the assistance of co-catalysts, participate in photoreduction or photooxidation reactions with absorbed reactants. Porphyrin/g-C₃N₄ composites have been extensively studied for solar energy utilization and conversion, including photocatalytic hydrogen production, CO₂ reduction, and pollutant degradation. These composites exhibit improved visible light harvesting ability, enhanced separation efficiency of charge carriers, and long-term stability. In this section, we briefly review the applications of porphyrin/g-C₃N₄ composites in the aforementioned areas.

4.1. Photocatalytic Water Splitting for Hydrogen Generation

Hydrogen is a promising green energy with the highest energy density (140 MJ kg⁻¹), which is dramatically higher than that of traditional hydrocarbon fuels (40–50 MJ kg⁻¹) [67]. Thus, the generation of hydrogen from water splitting utilizing semiconductor and solar energy is an appealing and promising substitute for fossil fuel [68]. Water splitting involves generation of oxygen as one product and formation of hydrogen as the other (Equations (1) and (2)). The overall transformation (Equation (3)) is a multielectron route advanced by solar energy and semiconductors, the bandgap of the semiconductor should be at 1.23–3.23 eV and the CB potential should be higher than hydrogen electrode potential.





The photocatalysts comprising porphyrin/*g*-C₃N₄ composites enhance charge transfer, thereby accelerating the rate of hydrogen evolution. This section primarily focuses on the research related to hydrogen evolution utilizing porphyrin/*g*-C₃N₄ composites. Table 1 provides a summary of the advancements in hydrogen generation through water splitting using porphyrin/*g*-C₃N₄ composites.

Table 1. Summary of porphyrin/*g*-C₃N₄ composite photocatalysts for hydrogen evolution from water.

Composite	Cocatalyst	Sacrificial Agent	Light Source	Activity	AQY	Ref.
C ₃ N ₄ /[(FeTPP) ₂ O]	N/A	10 vol% TEOA	300 W Xe Lamp	187.5 μmol g ⁻¹ h ⁻¹	0.0415% (420 nm)	[19]
ZnMT3PyP-Pt/C ₃ N ₄	Pt	50 mM AA	300 W Xe Lamp	2.28 mmol g ⁻¹ h ⁻¹	25.1% (420 nm)	[20]
TCPP/Pt/ <i>g</i> -C ₃ N ₄	Pt	10 vol% TEOA	450 W Hg Lamp (λ > 380 nm)	1.21 mmol g ⁻¹ h ⁻¹	N/A	[21]
<i>m</i> TCPP/CN	Pt	20 mM EDTA	Mercury vapour lamp	2.28 mmol g ⁻¹ h ⁻¹	N/A	[24]
NP/ <i>g</i> -C ₃ N ₄	Pt	10 vol% TEOA	300 W Xe Lamp	2.29 mmol g ⁻¹ h ⁻¹	N/A	[26]
<i>g</i> -C ₃ N ₄ -Cu-TCPP	N/A	10 vol% TEOA	300 W Xe Lamp	1.67 mmol g ⁻¹ h ⁻¹	N/A	[28]
<i>g</i> -C ₃ N ₄ -Cu-THPP	N/A	10 vol% TEOA	300 W Xe Lamp	7.5 μmol h ⁻¹	N/A	[29]
Au-P/Fe-CN	N/A	20 vol% methanol	300 W Xe Lamp	3.17 mmol g ⁻¹ h ⁻¹	3.26% (420 nm)	[31]
<i>g</i> -CNU-TDPP	Pt	10 vol% TEOA	300 W Xe Lamp	7.6 mmol g ⁻¹ h ⁻¹	13.3% (450 nm)	[35]
HBCNN/CoPMOF	Pt	AA	225 W Xe Lamp	33.5 mmol g ⁻¹ h ⁻¹	N/A	[56]
C ₃ N ₄ /Co/PMOF	N/A	17 vol% TEOA	300 W Xe Lamp	1.81 mmol g ⁻¹ h ⁻¹	N/A	[57]
MOC-Py-Zn/ <i>g</i> -C ₃ N ₄	N/A	10 vol% TEOA	300 W Xe Lamp	10.3 mmol g ⁻¹ h ⁻¹	N/A	[63]
ZnPy-4-Pt/C ₃ N ₄	Pt	50 mM AA	300 W Xe Lamp	3.49 mmol g ⁻¹ h ⁻¹	32.3% (420 nm)	[68]

Oxidizing water to produce oxygen is a challenging process, and current research primarily focuses on the half reaction of hydrogen evolution (Equations (1)–(3)). Alongside the photocatalyst and solar energy, sacrificial agents play a crucial role in harvesting unreacted holes to facilitate proton reduction, while co-catalysts are necessary under specific reaction conditions (Figure 20). Table 1 demonstrates that among the sacrificial agents, triethanolamine (TEOA) has proven to be the most efficient and widely employed for hydrogen generation. Additionally, when porphyrin molecules are combined with *g*-C₃N₄ photocatalysts, the assistance of co-catalyst Pt is generally required to achieve excellent hydrogen evolution activity. In the case of porphyrin/*g*-C₃N₄ Z-scheme systems, the presence of Pt as a co-catalyst is typically unnecessary due to their unique electron-hole transport mode and the higher reduction ability of their corresponding CB. As depicted in Table 1, the photocatalytic activities are commonly evaluated by measuring the hydrogen evolution rate, which often reaches up to mmol per gram of porphyrin/*g*-C₃N₄ composites within one hour. To account for variations in experimental instruments and other conditions, the apparent quantum efficiency (AQY) is also employed to assess the performance of photocatalysts and measure the efficiency of solar energy utilization.

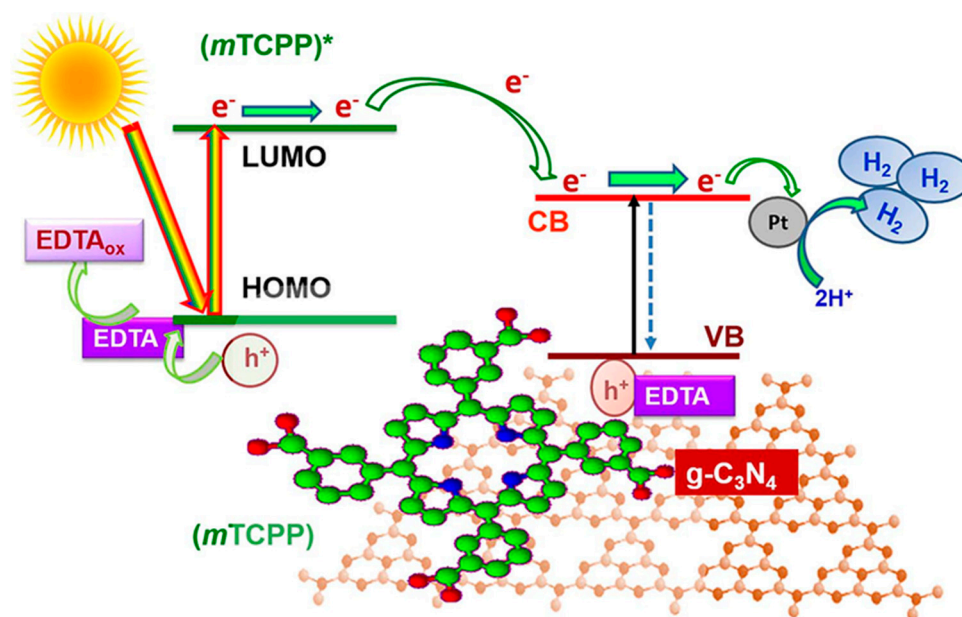
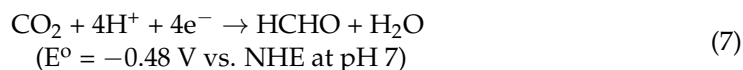
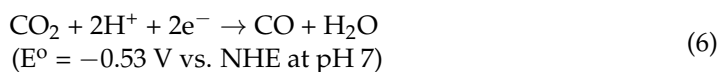
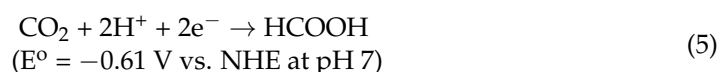
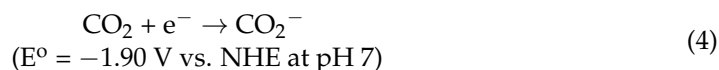
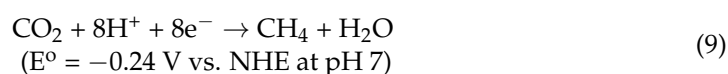
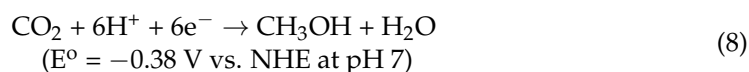


Figure 20. Proposed mechanism for photocatalytic hydrogen production from water over $g\text{-C}_3\text{N}_4$ sensitized with $m\text{TCPP}$, the $(m\text{TCPP})^*$ means the excited state of $m\text{TCPP}$. Reproduced from [24] with permission from [Elsevier].

4.2. Photocatalytic CO_2 Reduction

CO_2 is an integral part of the atmosphere and plays a crucial role in the global carbon cycle. The continuously increasing concentration of CO_2 , resulting from the explosive growth of the world's population and economic activities, has led to global warming and ecological changes due to its status as a leading greenhouse gas. Global energy demand, including fossil fuels, which are the main sources of CO_2 emissions, will continue to grow for a certain period. Inspired by natural photosynthesis, the photocatalytic reduction of CO_2 to reduce fuels such as methane, carbon monoxide, methanol, and other valuable chemicals has been recognized as a promising approach to address energy and environmental issues. This approach achieves two goals simultaneously [69,70]. However, the linear molecular geometry and the high bond energy of $\text{C}=\text{O}$ present certain challenges to CO_2 reduction, both from thermodynamic and dynamic perspectives. Similar to photocatalytic water splitting, photocatalytic CO_2 reduction also involves both the CO_2 reductive half-reaction and the water oxidative half-reaction in order to achieve carbon neutrality. The single-electron reduction of CO_2 requires extremely high energy, as shown in Equation (4). Therefore, the half-reaction typically follows a proton-assisted multi-electron pathway. The process involves the gradual acquisition of multiple electrons and hydrogen radicals to produce gaseous and liquid products such as CH_4 , CO , HCHO , and CH_3OH , as presented in Equations (5)–(9) [71].





The selectivity of the reduced products is primarily influenced by the structures of the photocatalyst. Hybrid heterojunctions between porphyrin and g-C₃N₄ have been extensively utilized for CO₂ reduction. The photocatalytic performance, including activity and selectivity, is summarized in Table 2.

Table 2. Summary of porphyrin/g-C₃N₄ composite photocatalysts for photocatalytic CO₂ reduction.

Composite	Reaction Solvent	Sacrificial Agent	Light Source	Activity	Ref.
g-C ₃ N ₄ /0.75% FeTCPP	CH ₃ CN:H ₂ O = 3:1	20 vol% TEOA	300 W Xe Lamp	CO: 1.09 mmol g ⁻¹ h ⁻¹	[22]
CNQD-[Fe- <i>p</i> -TMA]	H ₂ O	TEOA	Hg-Xe Lamp (55 mW cm ⁻²)	CO: 279 μmol h ⁻¹ TON: >10 ⁵ Selectivity: 96%	[27]
g-C ₃ N ₄ -CDs/FeTCPP	CH ₃ CN:H ₂ O = 3:1	20 vol% TEOA	300 W Xe Lamp	CO: 11.85 mmol g ⁻¹ h ⁻¹ CO: 17 μmol g ⁻¹ h ⁻¹	[30]
Co-porphyrin/g-C ₃ N ₄	CH ₃ CN	20 vol% TEOA	300 W Xe Lamp	CH ₄ : 0.7 μmol g ⁻¹ h ⁻¹ Selectivity: 80%	[33]
g-CNU-CoTDPP	CH ₃ CN	20 vol% TEOA	300 W Xe Lamp	CO: 57 μmol g ⁻¹ h ⁻¹ H ₂ : 14.2 μmol g ⁻¹ h ⁻¹ Selectivity: 79%	[36]
g-CNQDs/PMOF	CH ₃ CN:H ₂ O = 3:1	20 vol% TEOA	300 W Hg Lamp	CO: 16.1 μmol g ⁻¹ h ⁻¹ CH ₄ : 6.86 μmol g ⁻¹ h ⁻¹ Selectivity: 70%	[53]
Cu-Zn-TCPP/g-C ₃ N ₄	N/A	TEA	300 W Xe Lamp	CO: 43.75 μmol g ⁻¹ h ⁻¹ CH ₄ : 323.75 μmol g ⁻¹ h ⁻¹ CH ₄ selectivity: 88%	[54]
3% TCPP-C ₃ N ₄	N/A	H ₂ O	300 W Xe Lamp	CO: 16.8 μmol g ⁻¹ h ⁻¹ O ₂ : 10 μmol g ⁻¹ h ⁻¹	[60]

As can be seen, the photocatalytic reduction of CO₂ primarily occurs in either the liquid or gas phase. In the liquid phase reaction, the photocatalyst is uniformly dispersed in a CO₂-saturated solution. In the gas-phase reaction system, on the other hand, the photocatalyst is typically fixed on a substrate support, and a mixture of CO₂ and water vapor directly reacts with the photocatalyst. In the liquid phase reaction, sacrificial agents such as TEOA and triethylamine (TEA) are essential in the CO₂ reductive half-reactions to consume excessive generated holes, similar to the half-reaction in photocatalytic water splitting. Acetonitrile (CH₃CN) is often chosen as the solvent in the reaction system for two reasons: (1) Organic solvents have higher solubility for CO₂ gas compared to water, and (2) Competitive hydrogen evolution reactions can be effectively inhibited. Additionally, a certain amount of water is necessary as it can supply protons for participation in the proton-coupled multi-electron reduction of CO₂. The gas-phase reaction is independent of the solvent and sacrificial agent and represents a relatively simple reaction system. In porphyrin/g-C₃N₄ hybrid photocatalysts, g-C₃N₄ typically acts as a photosensitizer to absorb visible light and generate electrons, while porphyrin, particularly metal porphyrin, with metal ions (such as Fe, Co) at the center of the porphyrin ring, serves as the catalytic active site for reducing the adsorbed CO₂ to reduced products (Figure 21). However, there are exceptions, such as in the case of Cu-Zn-TCPP/g-C₃N₄ photocatalyst, where the Cu node in the 2D-MOF moiety is hydroxylated and functions as the catalytic center instead of the Zn ion in the porphyrin ring. In another case, the 2D-2D heterojunction TCPP nanosheets/C₃N₄ nanosheets catalyzes the overall CO₂ reduction without the addition of

sacrificial agents, with the porphyrin TCPP serving as a water oxidation booster and the C_3N_4 nanosheets acting as the CO_2 reduction center. Regarding the selectivity of products, CO is the main reduction product when employing porphyrin/ $g-C_3N_4$ nanocomposites as photocatalysts. In summary, current research based on porphyrin/ $g-C_3N_4$ nanocomposites for CO_2 reduction is still in its initial stages, requiring further progress in fabricating more efficient photocatalysts and understanding the mechanism of CO_2 reduction.

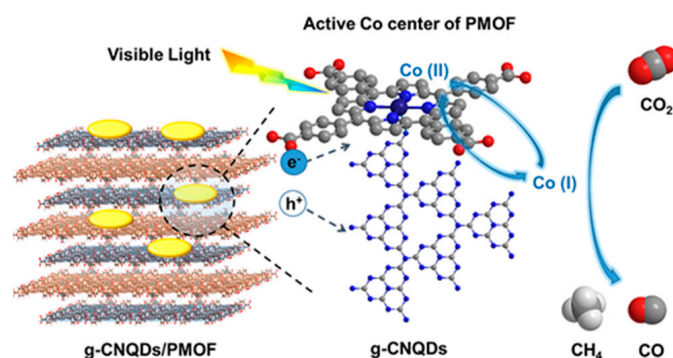


Figure 21. Proposed mechanism of CO_2 reduction over $g-CNQDs/PMOF$ hybrids under visible light irradiation. Reproduced from [53] with permission from [American Chemical Society].

4.3. Photocatalytic Degradation of Pollutants

With the global process of industrialization and the increasing global population, a significant amount of pollutants has been generated and discharged into the environment. This has raised concerns worldwide about sustainability because these pollutants not only contaminate the environment but also pose a threat to human health and well-being. In order to protect our environment and ensure the sustainable development of humanity, photocatalytic degradation of pollutants has emerged as an effective approach to harness solar energy and achieve these goals.

Porphyrin/ $g-C_3N_4$ hybrid photocatalysts possess the ability to efficiently absorb solar energy and facilitate rapid charge carrier transfer [72,73]. Consequently, they can be utilized to enhance the performance of photocatalytic pollutant degradation. The recent advancements in this field are summarized in Table 3.

Table 3. Summary of porphyrin/ $g-C_3N_4$ composite photocatalysts for photocatalytic pollutant degradation.

Composite	Light Source	Decomposition Rate	Initial Concentration	Ref.
CoTPP/ $g-C_3N_4$	350 W Xe Lamp	RhB: 99.79% in 90 min	25 $\mu\text{mol L}^{-1}$	[25]
O- $C_3N_4@(\text{Pd-TPyP})_3$	320W Xe Lamp	RhB: about 90% in 40 min	10 mg L^{-1}	[32]
ZnTCPP/ $g-C_3N_4$	300 W Xe Lamp	RhB: 96% in 30 min TC: 80.3% in 120 min	RhB: 10 mg L^{-1} TC: 30 mg L^{-1}	[34]
Co-porphyrin/ $g-C_3N_4$	300 W Xe Lamp	RhB: 97.9% in 120 min Ofloxacin: 95.9% in 200 min	20 mg L^{-1}	[55]
CuPor-Ph-COF/ $g-C_3N_4$	300 W Xe Lamp	RhB: 86% in 90 min	10 mg L^{-1}	[58]
SA-TCPP/O-CN	500 W Xe Lamp	BPA: 0.150 h^{-1}	10 ppm	[59]
$C_3N_4/TCPP$	350 W Xe Lamp	RhB: 0.033 min^{-1}	10 ppm	[61]
C_3N_4 -TCPP/CP	300 W Xe Lamp	RhB: 95% in 150 min	50 mg L^{-1}	[72]
0.1% TCPP/ $g-C_3N_4$	Xe Lamp	RhB: 0.033 min^{-1}	22 ppm	[73]

Figure 22 provides a schematic illustration of the photocatalytic degradation of pollutants based on porphyrin/ $g-C_3N_4$. Under light irradiation, photo-induced electrons typically migrate from the LUMO of porphyrin to the CB of $g-C_3N_4$ due to the more negative potential of the LUMO orbit of porphyrin. Conversely, holes preferentially transfer

from the VB of $g\text{-C}_3\text{N}_4$ to the HOMO orbit of porphyrin due to the more positive position of the CB of $g\text{-C}_3\text{N}_4$. The photo-induced electrons tend to react with oxygen molecules absorbed on the $g\text{-C}_3\text{N}_4$ surface, generating superoxide anion radicals ($\cdot\text{O}_2^-$), which contribute to the degradation of pollutants. Meanwhile, the generated holes tend to react with absorbed OH^- groups on the surface of porphyrin, producing hydroxyl radicals ($\cdot\text{OH}$) that facilitate pollutants degradation. As shown in Table 3, the catalytic performance of the photocatalysts was commonly evaluated using pollutants such as RhB, tetracycline (TC), and bisphenol A (BPA). The photocatalytic activities were typically assessed based on the decomposition rate of pollutants within a specified time or the apparent rate constant. The porphyrin/ $g\text{-C}_3\text{N}_4$ composite photocatalysts consistently exhibited significantly improved photocatalytic degradation performance compared to pristine $g\text{-C}_3\text{N}_4$. This enhancement can be attributed to the constructed heterojunctions, which not only enhance the separation and transportation of photo-generated charge carriers but also contribute to more efficient utilization of solar energy.

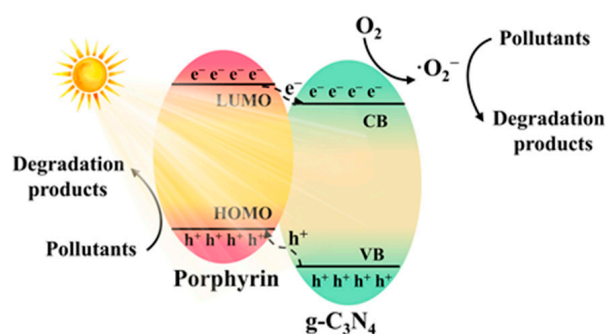


Figure 22. Proposed carrier separation, transfer route of porphyrin/ $g\text{-C}_3\text{N}_4$ composite, and photocatalytic pollution degradation process.

5. Challenges and Perspectives

Solar energy offers a distinct and natural advantage as a sustainable energy source. It is a renewable and abundant energy that endures over time and is widely accessible. Additionally, it is a completely clean, safe, and reliable energy source, not constrained by mining, transportation, or storage limitations. The most promising approach for solar energy conversion and storage involves chemical bonds. The development of new materials is necessary to harness and convert solar energy effectively. Porphyrin/ $g\text{-C}_3\text{N}_4$ composite photocatalysts have been designed and utilized for capturing solar energy across a broader spectrum and facilitating the separation of photo-generated charges. These catalysts have been successfully employed in photocatalytic hydrogen evolution, CO_2 reduction, and pollutant degradation. Despite notable progress, research in this field is still in its early stages, and several challenges remain to be addressed.

- (1) Although the porphyrin/ $g\text{-C}_3\text{N}_4$ composites broaden the absorption range of visible light, there is a need to further increase their utilization of higher-wavelength solar energy ($\lambda > 500$ nm).
- (2) The efficiency of separating photo-induced charges should be substantially enhanced as the current efficiency of the porphyrin/ $g\text{-C}_3\text{N}_4$ hybrid falls short of practical application requirements.
- (3) Fabrication of uniform single-layer or few-layer porphyrin/ $g\text{-C}_3\text{N}_4$ photocatalysts is necessary to achieve more efficient solar-to-chemical conversion and energy storage.
- (4) Addressing the challenge of oxygen evolution is crucial for both water splitting and CO_2 reduction. The scarcity of cocatalysts with high activity for oxygen evolution necessitates additional efforts.
- (5) The mechanism, cocatalysts, reaction pathways, and product selectivity involved in CO_2 reduction catalyzed by porphyrin/ $g\text{-C}_3\text{N}_4$ photocatalysts remain unclear and require further exploration and research.

- (6) The degradation of pollutants using porphyrin/g-C₃N₄ hybrid photocatalysts is still in its preliminary stages, and the photocatalytic degradation of gaseous pollutants has received less attention compared to organic pollutants in water.
- (7) The stability and recyclability of porphyrin/g-C₃N₄ photocatalysts are essential to meet industrial requirements and should be optimized for practical applications in the future.

Looking ahead to the future, porphyrin/g-C₃N₄ nano hybrids hold immense potential for applications in the field of artificial photosynthesis. This review aims to provide valuable insights and assistance for future research, fostering significant advancements in solar energy conversion. Progress in the design and synthesis of porphyrin/g-C₃N₄ materials will contribute to addressing the energy and environmental challenges we face. Collaborative efforts are essential to propel the practical utilization of porphyrin/g-C₃N₄ nanostructures, catalyzing a transformation in renewable energy. The realization of clean energy and environmental goals, achieved through the efficient production of carbon-neutral fuels via artificial photocatalysis, is no longer a distant dream but an achievable reality.

Funding: This work was financially supported by the National Natural Science Foundation of China (NSFC) U21A2085; Zhongyuan high level talents special support plan 204200510009; Scientific and Technological Innovation Team in University of Henan Province 20IRTSTHN001.

Conflicts of Interest: The authors declare no conflict of interest.

Sample Availability: Not applicable.

References

1. Lewis, N.S.; Nocera, D.G. Powering the planet: Chemical challenges in solar energy utilization. *Proc. Natl. Acad. Sci. USA* **2006**, *103*, 15729–15735. [[CrossRef](#)] [[PubMed](#)]
2. Zhang, P.; Wang, T.; Chang, X.; Gong, J. Effective Charge Carrier Utilization in Photocatalytic Conversions. *Acc. Chem. Res.* **2016**, *49*, 911–921. [[CrossRef](#)] [[PubMed](#)]
3. Ye, W.; Long, R.; Huang, H.; Xiong, Y. Plasmonic nanostructures in solar energy conversion. *J. Mater. Chem. C* **2017**, *5*, 1008–1021. [[CrossRef](#)]
4. Roy, S.C.; Varghese, O.K.; Paulose, M.; Grimes, C.A. Toward Solar Fuels: Photocatalytic Conversion of Carbon Dioxide to Hydrocarbons. *ACS Nano* **2010**, *4*, 1259–1278. [[CrossRef](#)]
5. Chen, X.; Shen, S.; Guo, L.; Mao, S.S. Semiconductor-based Photocatalytic Hydrogen Generation. *Chem. Rev.* **2010**, *110*, 6503–6570. [[CrossRef](#)]
6. Ben-Shahar, Y.; Stone, D.; Banin, U. Rich Landscape of Colloidal Semiconductor-Metal Hybrid Nanostructures: Synthesis, Synergetic Characteristics, and Emerging Applications. *Chem. Rev.* **2023**, *123*, 3790–3851. [[CrossRef](#)]
7. Chen, C.; Ma, W.; Zhao, J. Semiconductor-mediated photodegradation of pollutants under visible-light irradiation. *Chem. Soc. Rev.* **2010**, *39*, 4206–4219. [[CrossRef](#)]
8. Wang, C.-C.; Li, J.-R.; Lv, X.-L.; Zhang, Y.-Q.; Guo, G. Photocatalytic organic pollutants degradation in metal-organic frameworks. *Energy Environ. Sci.* **2014**, *7*, 2831–2867. [[CrossRef](#)]
9. Wang, X.; Maeda, K.; Thomas, A.; Takanabe, K.; Xin, G.; Carlsson, J.M.; Domen, K.; Antonietti, M. A metal-free polymeric photocatalyst for hydrogen production from water under visible light. *Nat. Mater.* **2009**, *8*, 76–80. [[CrossRef](#)]
10. Ong, W.-J.; Tan, L.-L.; Ng, Y.H.; Yong, S.-T.; Chai, S.-P. Graphitic Carbon Nitride (g-C₃N₄)-Based Photocatalysts for Artificial Photosynthesis and Environmental Remediation: Are We a Step Closer to Achieving Sustainability? *Chem. Rev.* **2016**, *116*, 7159–7329. [[CrossRef](#)]
11. Deng, A.; Sun, Y.; Gao, Z.; Yang, S.; Liu, Y.; He, H.; Zhang, J.; Liu, S.; Sun, H.; Wang, S. Internal electric field in carbon nitride-based heterojunctions for photocatalysis. *Nano Energy* **2023**, *108*, 108228. [[CrossRef](#)]
12. Tang, C.; Cheng, M.; Lai, C.; Li, L.; Yang, X.; Du, L.; Zhang, G.; Wang, G.; Yang, L. Recent progress in the applications of non-metal modified graphitic carbon nitride in photocatalysis. *Coord. Chem. Rev.* **2023**, *474*, 214846. [[CrossRef](#)]
13. Chen, Y.; Cheng, M.; Lai, C.; Wei, Z.; Zhang, G.; Li, L.; Tang, C.; Du, L.; Wang, G.; Liu, H. The Collision between g-C₃N₄ and QDs in the Fields of Energy and Environment: Synergistic Effects for Efficient Photocatalysis. *Small* **2023**, *19*, 2205902. [[CrossRef](#)] [[PubMed](#)]
14. Zhu, Y.; Liu, Y.; Ai, Q.; Gao, G.; Yuan, L.; Fang, Q.; Tian, X.; Zhang, X.; Egap, E.; Ajayan, P.M.; et al. In Situ Synthesis of Lead-Free Halide Perovskite-COF Nanocomposites as Photocatalysts for Photoinduced Polymerization in Both Organic and Aqueous Phases. *ACS Mater. Lett.* **2022**, *4*, 464–471. [[CrossRef](#)]
15. Yin, X.-L.; Liu, J.; Jiang, W.-J.; Zhang, X.; Hu, J.-S.; Wan, L.-J. Urchin-like Au@CdS/WO₃ micro/nano heterostructure as a visible-light driven photocatalyst for efficient hydrogen generation. *Chem. Commun.* **2015**, *51*, 13842–13845. [[CrossRef](#)]

16. Poulos, T.L. Heme Enzyme Structure and Function. *Chem. Rev.* **2014**, *114*, 3919–3962. [[CrossRef](#)]
17. e Silva, R.C.; da Silva, L.O.; de Andrade Bartolomeu, A.; Brocksom, T.J.; de Oliveira, K.T. Recent applications of porphyrins as photocatalysts in organic synthesis: Batch and continuous flow approaches. *Beilstein J. Org. Chem.* **2020**, *16*, 917–955. [[CrossRef](#)]
18. Sheng, H.; Wang, J.; Huang, J.; Li, Z.; Ren, G.; Zhang, L.; Yu, L.; Zhao, M.; Li, X.; Li, G.; et al. Strong synergy between gold nanoparticles and cobalt porphyrin induces highly efficient photocatalytic hydrogen evolution. *Nat. Commun.* **2023**, *14*, 1528. [[CrossRef](#)]
19. Wang, D.H.; Pan, J.N.; Li, H.H.; Liu, J.J.; Wang, Y.B.; Kang, L.T.; Yao, J.N. Pure organic heterostructure of μ -oxo dimeric iron(III) porphyrin and graphitic- C_3N_4 for solar H_2 reduction from water. *J. Mater. Chem. A* **2016**, *4*, 290–296. [[CrossRef](#)]
20. Wang, J.; Zheng, Y.; Peng, T.; Zhang, J.; Li, R. Asymmetric Zinc Porphyrin Derivative-Sensitized Graphitic Carbon Nitride for Efficient Visible-Light-Driven H_2 Production. *ACS Sustain. Chem. Eng.* **2017**, *5*, 7549–7556. [[CrossRef](#)]
21. Mei, S.; Gao, J.; Zhang, Y.; Yang, J.; Wu, Y.; Wang, X.; Zhao, R.; Zhai, X.; Hao, C.; Li, R.; et al. Enhanced visible light photocatalytic hydrogen evolution over porphyrin hybridized graphitic carbon nitride. *J. Colloid Interface Sci.* **2017**, *506*, 58–65. [[CrossRef](#)]
22. Lin, L.; Hou, C.; Zhang, X.; Wang, Y.; Chen, Y.; He, T. Highly efficient visible-light driven photocatalytic reduction of CO_2 over g- C_3N_4 nanosheets/tetra(4-carboxyphenyl)porphyrin iron(III) chloride heterogeneous catalysts. *Appl. Catal. B* **2018**, *221*, 312–319. [[CrossRef](#)]
23. Liu, J.; Shi, H.; Shen, Q.; Guo, C.; Zhao, G. A biomimetic photoelectrocatalyst of Co-porphyrin combined with a g- C_3N_4 nanosheet based on π - π supramolecular interaction for high-efficiency CO_2 reduction in water medium. *Green Chem.* **2017**, *19*, 5900–5910. [[CrossRef](#)]
24. Da Silva, E.S.; Moura, N.M.; Neves, M.G.P.; Coutinho, A.; Prieto, M.; Silva, C.G.; Faria, J.L. Novel hybrids of graphitic carbon nitride sensitized with free-base meso-tetrakis(carboxyphenyl) porphyrins for efficient visible light photocatalytic hydrogen production. *Appl. Catal. B* **2018**, *221*, 56–69. [[CrossRef](#)]
25. Zhang, J.; Wang, A.; Zhao, W.; Li, C.; Chen, X.; Wang, Y.; Zhu, W.; Zhong, Q. Influence of metal-porphyrins on the photocatalysis of graphitic carbon nitride. *Dyes Pigm.* **2018**, *153*, 241–247. [[CrossRef](#)]
26. Li, L.; Bodedla, G.B.; Liu, Z.; Zhu, X. Naphthalimide-porphyrin hybridized graphitic carbon nitride for enhanced photocatalytic hydrogen production. *Appl. Surf. Sci.* **2020**, *499*, 143755. [[CrossRef](#)]
27. Mistry, L.; Le-Quang, L.; Masdeu, G.; Bjorkman, W.; Harelind, H.; Abrahamsson, M. Selective Photocatalytic Reduction of CO_2 -to- CO in Water using a Polymeric Carbon Nitride Quantum Dot/Fe-Porphyrin Hybrid Assembly. *ChemCatChem* **2022**, *14*, e202200897. [[CrossRef](#)]
28. Zhu, K.; Zhang, M.; Feng, X.; Qin, L.; Kang, S.-Z.; Li, X. A novel copper-bridged graphitic carbon nitride/porphyrin nanocomposite with dramatically enhanced photocatalytic hydrogen generation. *Appl. Catal. B* **2020**, *268*, 118434. [[CrossRef](#)]
29. Zhang, M.; Zhu, K.; Qin, L.; Kang, S.-Z.; Li, X. Enhanced electron transfer and photocatalytic hydrogen production over the carbon nitride/porphyrin nanohybrid finely bridged by special copper. *Catal. Sci. Technol.* **2020**, *10*, 1640–1649. [[CrossRef](#)]
30. Zhang, X.; Lin, L.; Qu, D.; Yang, J.; Weng, Y.; Wang, Z.; Sun, Z.; Chen, Y.; He, T. Boosting visible-light driven solar-fuel production over g- C_3N_4 /tetra(4-carboxyphenyl)porphyrin iron(III) chloride hybrid photocatalyst via incorporation with carbon dots. *Appl. Catal. B* **2020**, *265*, 118595. [[CrossRef](#)]
31. Humayun, M.; Ullah, H.; Cheng, Z.-E.; Tahir, A.A.; Luo, W.; Wang, C. Au surface plasmon resonance promoted charge transfer in Z-scheme system enables exceptional photocatalytic hydrogen evolution. *Appl. Catal. B* **2022**, *310*, 121322. [[CrossRef](#)]
32. Yang, Y.J.; Sun, B.W.; Qian, D.J.; Chen, M. Fabrication of multiporphyrin@g- C_3N_4 nanocomposites via Pd(II)-directed layer-by-layer assembly for enhanced visible-light photocatalytic activity. *Appl. Surf. Sci.* **2019**, *478*, 1027–1036. [[CrossRef](#)]
33. Zhao, G.; Pang, H.; Liu, G.; Li, P.; Liu, H.; Zhang, H.; Shi, L.; Ye, J. Co-porphyrin/carbon nitride hybrids for improved photocatalytic CO_2 reduction under visible light. *Appl. Catal. B* **2017**, *200*, 141–149. [[CrossRef](#)]
34. Ma, Z.; Zeng, C.; Hu, L.; Zhao, Q.; Yang, Q.; Niu, J.; Yao, B.; He, Y. A high-performance photocatalyst of ZnTCPP sensitized porous graphitic carbon nitride for antibiotic degradation under visible light irradiation. *Appl. Surf. Sci.* **2019**, *484*, 489–500. [[CrossRef](#)]
35. Tian, S.; Chen, S.; Ren, X.; Cao, R.; Hu, H.; Bai, F. Bottom-up fabrication of graphitic carbon nitride nanosheets modified with porphyrin via covalent bonding for photocatalytic H_2 evolution. *Nano Res.* **2019**, *12*, 3109–3115. [[CrossRef](#)]
36. Tian, S.; Chen, S.; Ren, X.; Hu, Y.; Hu, H.; Sun, J.; Bai, F. An efficient visible-light photocatalyst for CO_2 reduction fabricated by cobalt porphyrin and graphitic carbon nitride via covalent bonding. *Nano Res.* **2020**, *13*, 2665–2672. [[CrossRef](#)]
37. Schlachter, A.; Asselin, P.; Harvey, P.D. Porphyrin-Containing MOFs and COFs as Heterogeneous Photosensitizers for Singlet Oxygen-Based Antimicrobial Nanodevices. *ACS Appl. Mater. Interfaces* **2021**, *13*, 26651–26672. [[CrossRef](#)]
38. Wang, Z.; Sun, Q.; Liu, B.; Kuang, Y.; Gulzar, A.; He, F.; Gai, S.; Yang, P.; Lin, J. Recent advances in porphyrin-based MOFs for cancer therapy and diagnosis therapy. *Coord. Chem. Rev.* **2021**, *439*, 213945. [[CrossRef](#)]
39. Leng, F.; Liu, H.; Ding, M.; Lin, Q.-P.; Jiang, H.-L. Boosting Photocatalytic Hydrogen Production of Porphyrinic MOFs: The Metal Location in Metalloporphyrin Matters. *ACS Catal.* **2018**, *8*, 4583–4590. [[CrossRef](#)]
40. Lan, Y.-Q.; Liu, M.; Chen, Y.-J.; Huang, X.; Dong, L.-Z.; Lu, M.; Guo, C.; Yuan, D.; Chen, Y.; Xu, G.; et al. Porphyrin-Based COF 2D Materials: Variable Modification of Sensing Performances by Post-Metallization. *Angew. Chem. Int. Ed.* **2022**, *61*, e202115308.
41. Chen, M.; Li, H.; Liu, C.; Liu, J.; Feng, Y.; Wee, A.G.H.; Zhang, B. Porphyrin- and porphyrinoid-based covalent organic frameworks (COFs): From design, synthesis to applications. *Coord. Chem. Rev.* **2021**, *435*, 213778. [[CrossRef](#)]

42. Zhang, X.-H.; Xu, Y.-S.; Qiao, Z.-Y.; Wang, H. Covalent organic frameworks (COFs) for photothermal therapy. *RSC Nanosci. Nanotechnol.* **2022**, *54*, 286–304.
43. Cao, R.; Wang, G.; Ren, X.; Duan, P.-C.; Wang, L.; Li, Y.; Chen, X.; Zhu, R.; Jia, Y.; Bai, F. Self-Assembled Porphyrin Nanoleaves with Unique Crossed Transportation of Photogenerated Carriers to Enhance Photocatalytic Hydrogen Production. *Nano Lett.* **2022**, *22*, 157–163. [[CrossRef](#)] [[PubMed](#)]
44. Liu, Y.; Wang, L.; Feng, H.; Ren, X.; Ji, J.; Bai, F.; Fan, H. Microemulsion-assisted self-assembly and synthesis of size-controlled porphyrin nanocrystals with enhanced photocatalytic hydrogen evolution. *Nano Lett.* **2019**, *19*, 2614–2619. [[CrossRef](#)]
45. Wang, J.; Zhong, Y.; Wang, X.; Yang, W.; Bai, F.; Zhang, B.; Alarid, L.; Bian, K.; Fan, H. pH-dependent assembly of porphyrin-silica nanocomposites and their application in targeted photodynamic therapy. *Nano Lett.* **2017**, *17*, 6916–6921. [[CrossRef](#)]
46. Zhong, Y.; Wang, Z.; Zhang, R.; Bai, F.; Wu, H.; Haddad, R.; Fan, H. Interfacial Self-Assembly Driven Formation of Hierarchically Structured Nanocrystals with Photocatalytic Activity. *ACS Nano* **2014**, *8*, 827–833. [[CrossRef](#)]
47. Jing, J.; Li, J.; Su, Y.; Zhu, Y. Non-covalently linked donor-acceptor interaction enhancing photocatalytic hydrogen evolution from porphyrin assembly. *Appl. Catal. B* **2023**, *324*, 122284. [[CrossRef](#)]
48. Yang, J.; Jing, J.; Li, W.; Zhu, Y. Electron Donor-Acceptor Interface of TPPS/PDI Boosting Charge Transfer for Efficient Photocatalytic Hydrogen Evolution. *Adv. Sci.* **2022**, *9*, 2201134. [[CrossRef](#)]
49. Zhang, Y.; Pan, C.; Bian, G.; Xu, J.; Dong, Y.; Zhang, Y.; Lou, Y.; Liu, W.; Zhu, Y. H₂O₂ generation from O₂ and H₂O on a near-infrared absorbing porphyrin supramolecular photocatalyst. *Nat. Energy* **2023**, *8*, 361–371. [[CrossRef](#)]
50. Shi, L.; Yang, L.; Zhang, H.; Chang, K.; Zhao, G.; Kako, T.; Ye, J. Implantation of Iron(III) in porphyrinic metal organic frameworks for highly improved photocatalytic performance. *Appl. Catal. B* **2018**, *224*, 60–68. [[CrossRef](#)]
51. Son, H.-J.; Pac, C.; Kang, S.O. Inorganometallic Photocatalyst for CO₂ Reduction. *Acc. Chem. Res.* **2021**, *54*, 4530–4544. [[CrossRef](#)] [[PubMed](#)]
52. Xia, Q.; Yang, J.; Zhang, S.; Zhang, J.; Li, Z.; Wang, J.; Chen, X. Bodipy-Based Metal-Organic Frameworks Transformed in Solid States from 1D Chains to 2D Layer Structures as Efficient Visible Light Heterogeneous Photocatalysts for Forging C-B and C-C Bonds. *J. Am. Chem. Soc.* **2023**, *145*, 6123–6134. [[CrossRef](#)]
53. Zheng, C.; Qiu, X.; Han, J.; Wu, Y.; Liu, S. Zero-Dimensional-g-CNQD-Coordinated Two-Dimensional Porphyrin MOF Hybrids for Boosting Photocatalytic CO₂ Reduction. *ACS Appl. Mater. Interfaces* **2019**, *11*, 42243–42249. [[CrossRef](#)] [[PubMed](#)]
54. Xie, S.; Deng, C.; Huang, Q.; Zhang, C.; Chen, C.; Zhao, J.; Sheng, H. Facilitated Photocatalytic CO₂ Reduction in Aerobic Environment on a Copper-Porphyrin Metal-Organic Framework. *Angew. Chem. Int. Ed.* **2023**, *62*, e202216717.
55. Jia, H.; Ma, D.; Zhong, S.; Li, L.; Li, L.; Xu, L.; Li, B. Boosting photocatalytic activity under visible-light by creation of PCN-222/g-C₃N₄ heterojunctions. *Chem. Eng. J.* **2019**, *368*, 165–174. [[CrossRef](#)]
56. Pu, Z.; Xiao, B.; Mao, S.; Sun, Y.; Ma, D.; Wang, H.; Zhou, J.; Cheng, Y.; Shi, J.-W. An electron-hole separation mechanism caused by the pseudo-gap formed at the interfacial Co-N bond between cobalt porphyrin metal organic framework and boron-doped g-C₃N₄ for boosting photocatalytic H₂ production. *J. Colloid Interface Sci.* **2022**, *628*, 477–487. [[CrossRef](#)]
57. Zhou, Y.; Zhang, T.; Zhu, W.; Qin, L.; Kang, S.-Z.; Li, X. Enhanced light absorption and electron transfer in dimensionally matched carbon nitride/porphyrin nanohybrids for photocatalytic hydrogen production. *Fuel* **2023**, *338*, 127394. [[CrossRef](#)]
58. Hou, Y.; Cui, C.-X.; Zhang, E.; Wang, J.-C.; Li, Y.; Zhang, Y.; Zhang, Y.; Wang, Q.; Jiang, J. A hybrid of g-C₃N₄ and porphyrin-based covalent organic frameworks via liquid-assisted grinding for enhanced visible-light-driven photoactivity. *Dalton Trans.* **2019**, *48*, 14989–14995. [[CrossRef](#)]
59. Xu, J.; Gao, Q.; Wang, Z.; Zhu, Y. An all-organic 0D/2D supramolecular porphyrin/g-C₃N₄ heterojunction assembled via π - π interaction for efficient visible photocatalytic oxidation. *Appl. Catal. B* **2021**, *291*, 120059. [[CrossRef](#)]
60. Chen, Q.; Zhang, Y.; You, E.; Jiang, Q.; Chen, X.; Wang, Y.; Song, Z.; Chang, K.; Xie, Z.; Kuang, Q. Accelerated water oxidation kinetics triggered by supramolecular porphyrin nanosheet for robust visible-light-driven carbon dioxide reduction. *Small* **2022**, *18*, 2204924. [[CrossRef](#)]
61. Lai, H.T.; Nguyen, G.T.; Tran, N.T.; Nguyen, T.T.; Van Tran, C.; Nguyen, D.K.; Chang, S.W.; Chung, W.J.; Nguyen, D.D.; Thi, H.P.N.; et al. Assembled Porphyrin Nanofiber on the Surface of g-C₃N₄ Nanomaterials for Enhanced Photocatalytic Degradation of Organic Dyes. *Catalysts* **2022**, *12*, 1630. [[CrossRef](#)]
62. Zou, W.; Liu, X.-H.; Xue, C.; Zhou, X.-T.; Yu, H.-Y.; Fan, P.; Ji, H.-B. Enhancement of the visible-light absorption and charge mobility in a zinc porphyrin polymer/g-C₃N₄ heterojunction for promoting the oxidative coupling of amines. *Appl. Catal. B* **2021**, *285*, 119863. [[CrossRef](#)]
63. Lei, Y.; Huang, J.-F.; Li, X.-A.; Lv, C.-Y.; Hou, C.-P.; Liu, J.-M. Direct Z-scheme photochemical hybrid systems: Loading porphyrin-based metal-organic cages on graphitic-C₃N₄ to dramatically enhance photocatalytic hydrogen evolution. *Chin. J. Catal.* **2022**, *43*, 2249–2258. [[CrossRef](#)]
64. Kumar, S.G.; Devi, L.G. Review on modified TiO₂ photocatalysis under UV/Visible light: Selected results and related mechanisms on interfacial charge carrier transfer dynamics. *J. Phys. Chem. A* **2011**, *115*, 13211–13241. [[CrossRef](#)]
65. John, A.T.; George, D.; Hariharan, M. Charge Transport through Discrete Crystalline Architectures. *J. Phys. Chem. C* **2023**, *127*, 3389–3397. [[CrossRef](#)]
66. Kamat, P.V. Manipulation of Charge Transfer Across Semiconductor Interface. A Criterion That Cannot Be Ignored in Photocatalyst Design. *J. Phys. Chem. Lett.* **2012**, *3*, 663–672. [[CrossRef](#)]

67. Wang, Z.; Li, C.; Domen, K. Recent developments in heterogeneous photocatalysts for solar-driven overall water splitting. *Chem. Soc. Rev.* **2019**, *48*, 2109–2125. [[CrossRef](#)]
68. Zheng, Y.; Wang, J.; Zhang, J.; Peng, T.; Li, R. Syntheses of asymmetric zinc porphyrins bearing different pseudo-pyridine substituents and their photosensitization for visible-light-driven H₂ production activity. *Dalton Trans.* **2017**, *46*, 8219–8228. [[CrossRef](#)]
69. Albero, J.; Peng, Y.; Garcia, H. Photocatalytic CO₂ reduction to C₂+ products. *ACS Catal.* **2020**, *10*, 5734–5749. [[CrossRef](#)]
70. Chang, X.; Wang, T.; Gong, J. CO₂ photo-reduction: Insights into CO₂ activation and reaction on surfaces of photocatalysts. *Energy Environ. Sci.* **2016**, *9*, 2177–2196. [[CrossRef](#)]
71. Wang, X.; He, J.; Chen, X.; Ma, B.; Zhu, M. Metal halide perovskites for photocatalytic CO₂ reduction: An overview and prospects. *Coord. Chem. Rev.* **2023**, *482*, 215076. [[CrossRef](#)]
72. Shao, F.; Mi, L.; Tian, Z.; Zheng, C.; Zhang, Y.; Li, Q.; Liu, S. Promoting Photodegradation Efficiency via a Heterojunction Photocatalyst Combining with Oxygen Direct and Fast Diffusion from the Gas Phase to Active Catalytic Sites. *ACS Appl. Mater. Interfaces* **2019**, *11*, 44922–44930. [[CrossRef](#)] [[PubMed](#)]
73. Liu, S.; Zhou, S.; Hu, C.; Duan, M.; Song, M.; Huang, F.; Cai, J. Coupling graphitic carbon nitrides with tetracarboxyphenyl porphyrin molecules through π - π stacking for efficient photocatalysis. *J. Mater. Sci. Mater. Electron.* **2020**, *31*, 10677–10688. [[CrossRef](#)]

Disclaimer/Publisher's Note: The statements, opinions and data contained in all publications are solely those of the individual author(s) and contributor(s) and not of MDPI and/or the editor(s). MDPI and/or the editor(s) disclaim responsibility for any injury to people or property resulting from any ideas, methods, instructions or products referred to in the content.